2014

Variability of Cross-Slope Flow in the Desoto Canyon Region

Thanh Tam Nguyen

FLORIDA STATE UNIVERSITY

COLLEGE OF ARTS AND SCIENCES

VARIABILITY OF CROSS-SLOPE FLOW IN THE DESOTO CANYON REGION

By

THANH TAM NGUYEN

A Thesis submitted to the
Department of Earth, Ocean and Atmospheric Science
in partial fulfillment of the
requirements for the degree of
Master of Science

Degree Awarded:
Fall Semester, 2014

Thanh Tam Nguyen defended this thesis on September 24, 2014.
The members of the supervisory committee were:

Eric Chassignet
Professor Directing Thesis

William Dewar
Committee Member

Dmitry Dukhovskoy
Committee Member

Markus Huettel
Committee Member

Steven Morey
Committee Member

The Graduate School has verified and approved the above-named committee members, and certifies that the thesis has been approved in accordance with university requirements.

ACKNOWLEGMENTS

Foremost, I would like to thank my major advisor, Dr. Chassignet for his guidance and support through my studies at Florida State University. Dr. Chassignet taught me many lessons about conducting research and working with people, and enjoying my work. I would also like to thank the committee members, Drs. Dewar, Dukhovskoy, Huettel and Morey. They offered interesting scientific advice and discussions that helped guide me through my studies, in particular, Drs. Dukhovskoy and Morey, who were my daily advisors. Also I would like to thank Dr. Hiester, Dr. Morey, Mrs. Fearon and Mrs. Field for their help with scientific writing and editing.

My fellow graduate students and friends have shared great memories of learning and living in Tallahassee, in particular, Chi, David, Duygu, Giang, Hannah, Nghia, Rachel, Robbies, Rosangle, Russ, Tabitha and Tim. I learned a lot from them and appreciate their friendship.

Finally, I want to show my special gratitude to my family in Vietnam for their love and encouragement. They always support me to get through hard times and be confident with my decisions. This work is dedicated to them.

The research was supported by the Gulf of Mexico Research Initiative Deep-C Consortium, NOAA/NGI and ONR HYCOM.

TABLE OF CONTENTS

LIST OF FIGURES

ABSTRACT

Cross-slope flow is critical for governing heat and material exchange, including pollutants and biota, between the coastal and deep ocean. This study focuses on characterizing the variability of cross-slope near-bottom flow in the DeSoto Canyon region, where the BP's Macondo well exploded in April 2010, using a multi-decadal HYbrid Coordinate Ocean Model (HYCOM) simulation of Gulf of Mexico circulation. Due to change in shelf orientation east and west of the canyon, wind-driven vertical motions are mostly related to a component of the local wind vector along an angle that may deviate from the local isobaths, with smaller deviations from the along-isobath direction to the east of the canyon and bigger departures to the west. This implies that upwelling is associated with along-isobath winds east of the canyon but shelf waves propagating from the eastern shelf, where northwesterly winds are upwelling favorable, influence cross-slope flow to the west of the canyon. Beyond the shelf break, where the Loop Current and its eddies can directly impact the depth of isotherms, the isotherms are deepened underneath the Loop Current and anticyclones but uplifted on their inshore periphery. The Loop Current also interacts with the west Florida shelf and generates a high pressure gradient that extends northward along the continental slope into the study domain. Consequently, large-scale and persistent upwelling and downwelling events take place over the continental slope of the domain. The vertical excursions mostly range from ±35 to ± 50 m for the shallow isopycnals but can reach to over ± 100 m. Most distinct upwelling and downwelling events are short duration on the order of days, however there is a significant chance for persistent events, which can be induced by either remote or direct interaction of the Loop Current and/or eddies with the slope.

CHAPTER 1

INTRODUCTION

Upwelling and downwelling are common oceanic phenomena that play important roles in biological productivity and chemical cycling in the oceans. Upwelling and downwelling can occur in both coastal areas and in the open ocean. Although the upwelling process covers only a small portion of the ocean's surface, it accounts for about eighty to ninety percent of the world's new biological production and greater than ninety-five percent of the sedimentary accumulation of organic carbon (Brink et al., 1995). Upwelling is also associated with the world's major fisheries, including those in the waters off northwestern Africa and the Iberian Peninsula; southwestern Africa, Peru and Chile, and Oregon and California, as well as in the Arabian Sea.

Upwelling and downwelling are mainly driven by winds and thus typically change seasonally. In spring and summer, northerly winds blowing along the coasts of Oregon and California and southerly winds along the coasts of Chile and Peru generate offshore Ekman transport of surface waters that is compensated for by onshore transport of subsurface waters up the continental slope. In contrast, in winter winds blowing in the opposite direction can generate onshore surface Ekman transport, causing convergence and consequently downwelling close to the coast. Tropical easterlies can drag the surface water westward along the Equator. The rotation of the Earth can deflect this flow to the right in the northern hemisphere and to the left in the southern hemisphere. When surface waters are driven away from the Equator, upwelling takes place.

Upwelling and downwelling are essential for mixing and distributing heat, oxygen, and nutrients in the ocean. In upwelling systems, the upward vertical motion of water can bring substances from the deeper layers of the ocean to the surface. These substances include nutrients such as nitrate, silica, and phosphate that stimulate blooms of phytoplankton and seaweed as they rise to the euphotic zone. Accordingly, high productivity zones are likely to form in upwelling systems. On the other hand, downwelling processes are related to low productivity regions but are important for bottom-dwelling sea life. The processes help to renew waters and dissolved oxygen in the near-bottom layers, preventing some benthic organisms from adverse conditions or even extinction. In addition, other substances including pollutants can be transported vertically in the water column, potentially leading to serious consequences for marine environments and organisms in both the long and short term.

1.1 Motivation

Recently, increased human activities in coastal and marine areas have resulted in pollution that seriously threatens marine ecosystems and environments. The Gulf of Mexico is a prime area for the extraction and production of oil and gas, industrial and recreational fisheries, and maritime transport. The explosion of the British Petroleum Deepwater Horizon offshore drilling rig in the northeastern Gulf of Mexico on 20 April 2010 was the worst accidental oil spill in U.S. history. More than two hundred million gallons of crude oil from the Macondo well leaked into the Gulf of Mexico waters for approximately eighty-four days (Ramseur, 2010). This explosion polluted wide areas of the Gulf of Mexico, including the waters off Mississippi, Louisiana, Alabama, and Florida (Weisberg et al., 2014). When oil is released into waters, several processes that depend on atmospheric and oceanic conditions, such as dispersion, emulsification, adsorption, biodegradation, sedimentation, and photolysis, can occur. Winds and currents cause the oil slicks to drift on the surface and waves and winds influence oil-water mixing and oil emulsification. Oil droplets suspended in the water column can interact with sediment and sink to the ocean bottom. Impacts of the oil spill on marine species have been widely documented. For example 456 of 1,149 sea turtles collected during 2010–2011 were affected by oil; 600,000 to 800,000 coastal birds died; 577 pelicans were found to die in May 2011; more than 900 bottlenose dolphins were dead and stranded in the oil area in the period of 2010–2014; about 500 stranded sea turtles were affected by the spill every year from 2011 to 2013; bluefin tuna larval abundance was reduced to 20 % in 2010 as the oil can damage hearts of bluefin tuna, amberjack and yellowfin tuna (http://www.oceanconservancy.org/places/gulf-of-mexico/pdf-4-years-after-bp.pdf; National Wildlife Federal report, 2014).

A large amount of the oil spilled from the Deepwater Horizon disaster in the Gulf of Mexico remains unaccounted for, e.g. over 70% in August 2010, and much has presumably been deposited to the ocean floor through downwelling processes or sinking of suspended oiled sediments (Hopkinson, 2010). The oil in the deep ocean may have a devastating effect on the deep marine ecosystems. Strong deep currents have been observed in the deep Gulf (Hamilton and Lugo-Fernandez, 2001). These currents can resuspend and transport toxic sediments and oil residue over a large distance. It is also possible that the oiled sediment can be brought up to the surface and the shallower regions through upwelling processes (Weisberg et al., 2014). This mechanism may have played a role during Hurricane Isaac in 2012 when about 565,000 pounds

of oil residue traced to the Deepwater Horizon spill was brought to the Louisiana coast (Adelson, 2012). A close proximity to the oil spill location makes the northeastern Gulf shelf vulnerable to the threat of oil upwelled from the deep ocean. Particularly vulnerable are the regions close to the DeSoto Canyon that connects the deep ocean basin with the shelf areas.

Apart from the potential impacts of upwelling associated with the Deepwater Horizon disaster, persistent upwelling associated with cross-slope flows may substantially alter water properties and ecosystems on the shelf, as happened in the northeastern Gulf of Mexico in 1998 resulting in a mass fish mortality event (Collard and Lugo-Fernandez, 1999; Collard et al., 2000). Anomalous cooler and nutrient-rich waters were transported onto the continental shelf, providing favorable conditions for phytoplankton blooms and subsequently high demand of oxygen. Strong stratification due to high river inflows and rainfall during this period led to hypoxia in the shallow water. Consequently lethargic and dead fishes and invertebrates were observed at depths of 10–35 m over a large region.

Upwelling and downwelling induced by cross-slope flows are, therefore, important for material transport between coastal and deep ocean which, in turn, greatly influences marine environment and ecology. However, upwelling and downwelling is not well understood in the northeastern Gulf of Mexico, in particular, the governing mechanisms of these processes.

1.2 Goal and Objectives

The goals of this study are 1) to characterize upwelling and downwelling associated with cross-slope flows in the northeastern Gulf of Mexico and 2) to identify the major mechanisms that cause this upwelling and downwelling. A multi-decadal Gulf of Mexico HYbrid Coordinate Ocean Model (GoM-HYCOM) numerical simulation is used for this study. Appropriate metrics are developed to detect upwelling and downwelling events from the model outputs. Spatial and temporal distributions of the cross-slope flow are characterized and the mechanisms are determined. This study focuses on the roles of the wind, topographic waves and meso-scale circulation features and examines favorable conditions and hotspots for upwelling. This study contributes to a comprehensive picture of ocean circulation near the DeSoto Canyon, useful for local marine ecology and for management and response of any future contaminant releases in the northeastern Gulf of Mexico.

1.3 Structure

This thesis is organized into six chapters, and each chapter is summarized as follows:

Chapter 1 provides an introduction to general upwelling and downwelling in oceans and seas, the motivation for the study, and the goal and objectives for studying the cross-slope flow in the DeSoto Canyon region.

Chapter 2 reviews background information on the Gulf of Mexico, the DeSoto Canyon region and upwelling and downwelling processes.

Chapter 3 describes hypotheses of the major mechanisms governing the cross-slope flows.

Chapter 4 presents on the main dataset of the GoM-HYCOM simulation and study methods.

Chapter 5 discusses main results on wind- and mesoscale-induced upwelling and downwelling, and its characteristics.

Chapter 6 provides major conclusion and discussion.

In addition, the thesis has four appendices containing additional results.

CHAPTER 2

BACKGROUND

2.1 Circulation in the Gulf of Mexico

2.1.1 Large-scale Circulation

Circulation in the deeper regions of the Gulf of Mexico is dominated by the Loop Current and its associated eddies (Fig. 2-1). The Loop Current, part of the Gulf Stream, enters into the Gulf of Mexico through the Yucatan Chanel and exits east through the Straits of Florida. It provides the major source of energy and momentum for circulation in the Gulf of Mexico. When the Loop Current penetrates north and becomes sufficiently unstable, a large anticyclonic eddy gradually breaks off. These anticyclonic eddies are usually asymmetric with maximum speeds of 1.78 m/s and 1.32 m/s on their south and north edges, respectively (Forristal et al., 1992) and commonly have diameters of 200–300 km and lifetimes on the order of months (Oey et al., 2005). The separated anticyclone tends to drift to the west at approximately 3 to 6 km/day and then can break into smaller eddies, affecting flows over the continental shelf break and slope in the western Gulf (Hamilton and Lee, 2005).

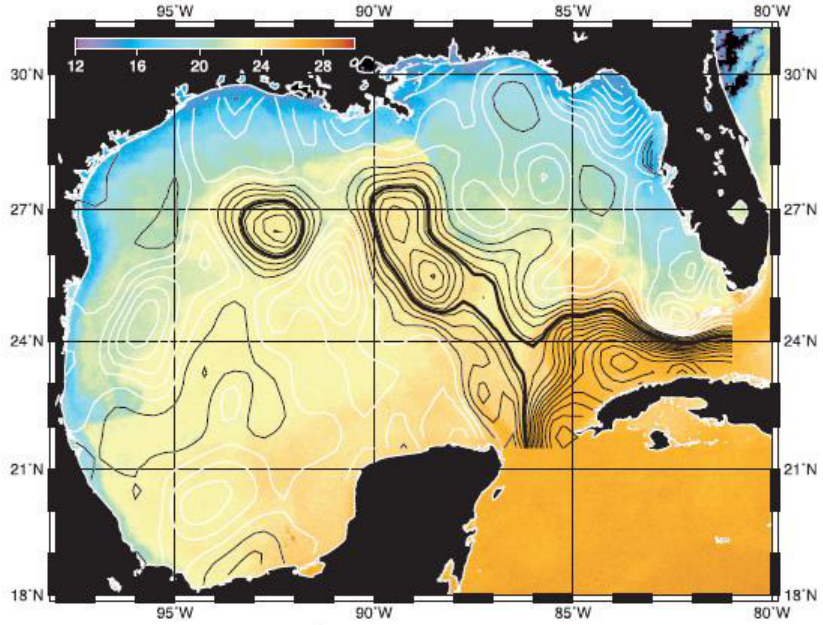

Figure 2-1: The Loop Current and its associated eddy field in the Gulf of Mexico. (Leben, 2005).

The Loop Current's eddy-shedding periods are thoroughly variable, ranging from several weeks to 18 or 19 months (Leben, 2005; Vukovich, 2012) (Fig. 2-2). Sturges and Leben (2000) found 44 consecutive eddy separation events in the period 1973 through 2004 and Vukovich (2012) documented 16 events during 2001–2010. They provided the distributions of the separation periods which peak at 6, 9 and 11 months (Fig. 2-2). Analysis of the altimeter-derived sea surface height (SSH) gridded field produced by the Colorado Center for Astrodynamics Research (CCAR) for the period 1993 through 2010 also reveals 27 eddy separation events. The mean eddy shedding period assessed from these data is about 8 months; the median is 6.47 months and the mode is 6–7 months (Fig. 2-3). This result is slightly different from the work of Vukovich (2012) who argues that a bimodal distribution of the separation periods has the mean of 10.2 months and the modes of 6 and 11 months during 1972–2010. After an eddy separation, the Loop Current retreats southward, and its location is shown to be linearly related to subsequent eddy separation (Leben, 2005).

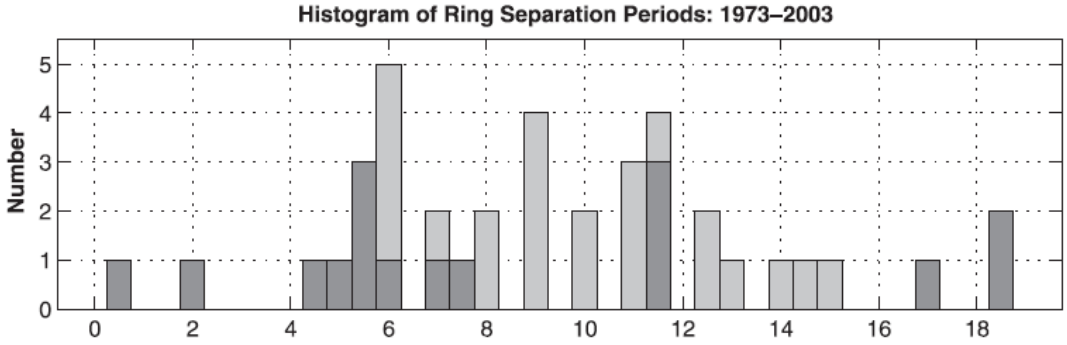

Figure 2-2: Histogram of ring separation periods. (Leben, 2005).

A spatial probability map of Loop Current water in the Gulf of Mexico was created from a 54-year Gulf of Mexico HYCOM simulation (GoM-HYCOM) (Dukhovskoy et al., 2014). Following Leben (2005), the Loop Current and Loop Current eddy front are tracked using the 0.17 m contour in demeaned SSH fields. Demeaned fields are calculated by subtracting the spatial mean from each daily SSH fields. Fig. 2-4 depicts the frequency of the Loop Current covering different water areas in the Gulf of Mexico. Typically the Loop Current is located south of 27°N and east of 88°W with approximately 50 % of the simulation time spent in these regions. It is rarer, < 5 % of the simulation time, that the Loop Current reaches north of 28°N as well as

west of 90°W. This finding is in agreement with previous observationally based studies (e.g. Vukovich et al., 1979; Huh et al., 1981; Sturges and Evans, 1983).

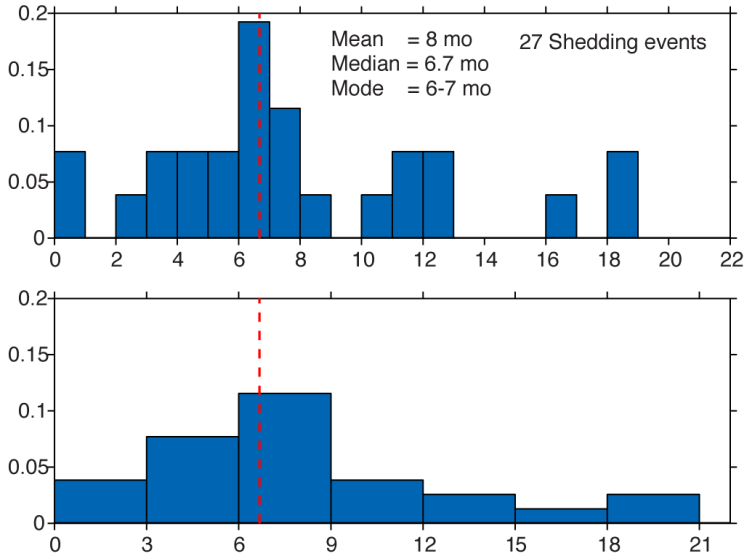

Figure 2-3: Normalized histograms of the Loop Current eddy separation period (months) from the altimeter-derived data (CCAR SSH fields) for 1993–2010. The vertical red dashed line is the median. The ordinate is normalized frequency (which multiplied by the bin size yields the occurrence probability of the Loop Current front within the bin's longitude and latitude range). The abscissa is the separation period. Top: 1-month binning. Bottom: 3-month binning. Estimates of the mean, median and mode of the separation periods are shown in the top panel. (courtesy of D. Dukhovskoy).

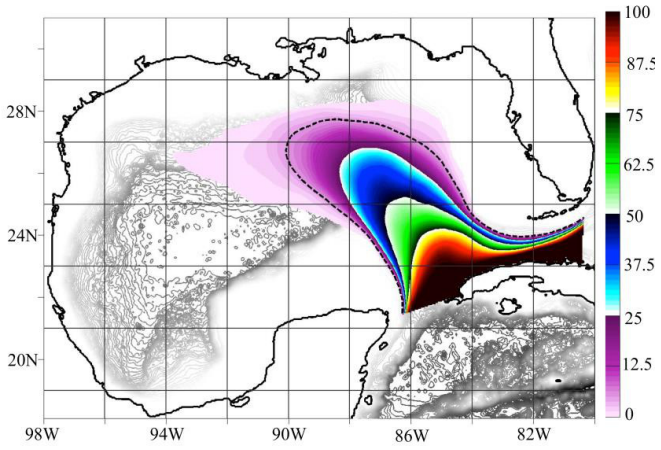

Figure 2-4: Spatial probability (percent) of grid cells being inside the Loop Current from the multi-decadal HYCOM simulation. The Loop Current is defined from a 7-day averaged SSH field. The dashed contour marks 5 % probability line and the map is thresholded at 0.25 %. Grey contours in the background indicate the isobaths. (courtesy of D. Dukhovskoy).

In particular, northern and western extensions of the 5 % probability contour (about 28 °N and 90 °W) are relatively consistent with Vukovich (2007), which is based on satellite and hydrographic data. The maximum westward and northward extent of the Loop Current of 93.1°W and 28.1°N, respectively, were derived from altimeter observations (Leben, 2005). From Fig. 2-4, it is apparent that the Loop Current is restricted to the deep basin, because of its vertical scale, on the order of 1000 m, which prevents its expansion over shallower regions. This is also true for the Loop Current eddies.

2.1.2 The West Florida Shelf and the Northeastern Gulf of Mexico

Continental shelf currents are dynamically complicated in the eastern Gulf of Mexico, especially in the DeSoto Canyon region. The shelf has dramatically varying width, radical curvature, and is subject to impingement of strong offshore currents, making this a region of special dynamic interest. Generally, coastal circulation exhibits seasonal variability and is governed by local winds and buoyancy fluxes due to river inflows and surface heat fluxes. In spite of large buoyancy gradients, coastal circulation is principally wind-induced, especially on the inner shelf (Weisberg et al., 2001; He and Weisberg, 2003; Morey et al., 2005). Cragg et al. (1983) analyzed tidal and meteorological data records along the Gulf coast from St. Petersburg through Pensacola and demonstrated that flow patterns and sea level variations are strongly correlated with local wind stresses. Wind speed of 4 m/s here can result in approximately 16 cm variation of sea level over a wide range of 4–10 days. Marmorino et al. (1983) confirmed a strong relationship between flows and wind stresses through mooring data in the northeastern Gulf of Mexico in the wintertime of 1981–1982. Winds parallel to the coast are capable of generating a mean alongshore velocity of 40 cm/s and a cross-shelf near-bottom flow on the continental shelf off Cape San Blas.

Morey et al. (2005) and Weisberg et al. (2005) showed that along-shelf wind-driven flows on the inner and middle shelves of the DeSoto Canyon region are upcoast (with the coast to the left in the northern hemisphere) during winter and spring and downcoast during summer and fall (Figs. 2-5 and 2-6). However, there are reversal flows at the shelf break and on the outer shelf, with northwestward flow in winter and southeastward flow in summer. The continental shelf flows in the DeSoto Canyon region are stronger than those in the Florida Big Bend and south of the west Florida shelf. Moreover, low-frequency, along-isobath flows in the Big Bend region

were found to be impacted by both the local along-isobath wind stress and the southward wind stress along the west Florida shelf based on in situ measurements at the 19-m station, and to be weakened by an alongshore pressure gradient propagating northward as a coastally trapped wave (Maksimova and Clarke, 2013). The low-frequency flows were also observed to be locally wind-driven in water depth of 5 m (ibid.).

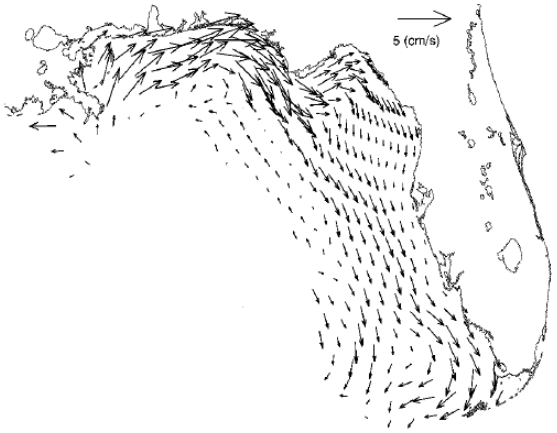

Figure 2-5: Seasonal mean depth-averaged flow induced by local winds during spring. (Weisberg et al., 2005).

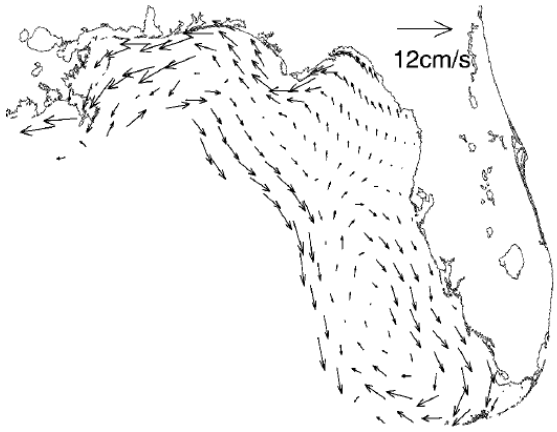

Figure 2-6: Seasonal mean depth-averaged flow induced by local winds during fall. (Weisberg et al., 2005).

Within close proximity to the continental slope, mesoscale circulation features greatly impact circulation on the outer shelf (Hsueh and Golubev, 2002; Hsueh and Weisberg, 2002; He and Weisberg, 2003). Numerical barotropic experiments by He and Weisberg (2003) with an idealized Loop Current forcing showed that when the Loop Current comes into contact with the central portion of the west Florida shelf, it can cause a shelf break jet that extends from the Mississippi River to south of the west Florida shelf (Fig. 2-7). This jet is associated with a Loop Current-induced high pressure anomaly extending along the continental slope, consistent with Hetland et al. (1999). In the DeSoto Canyon region, the jet is northeastward over the outer slope on the seaward (western) side of the high pressure anomaly and southeastward along the eastern side (Hetland et al., 1999). The jet extends inshore on the narrow shelf of the DeSoto Canyon (Chapman and Brink, 1987; He and Weisberg, 2003). In addition, Hetland et al. (1999) found that when the contact point of the Loop Current is located at the southeastern corner of the west Florida shelf, the southward jet tends to expand onto the continental shelf.

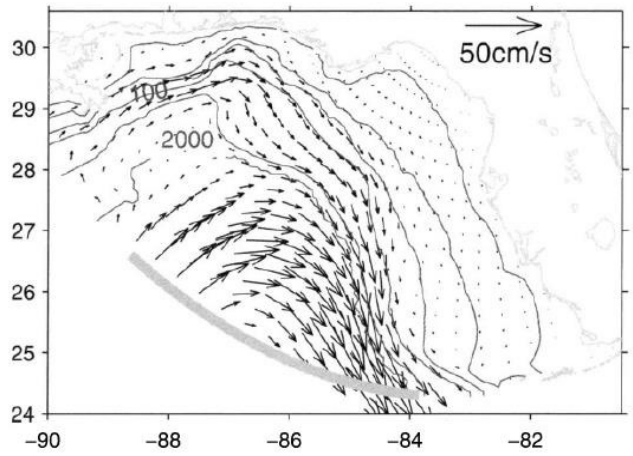

Figure 2-7: Depth-averaged flow numerically simulated by the idealized Loop Current. (He and Weisberg, 2003).

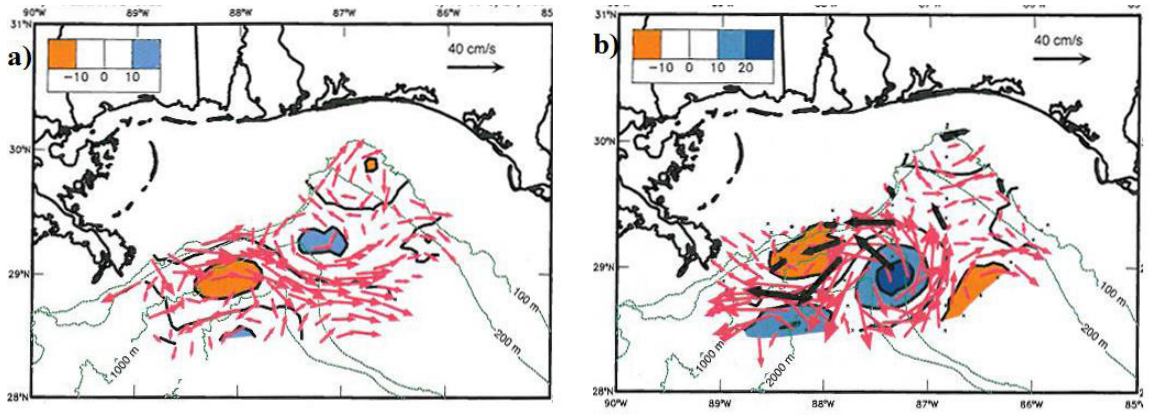

Figure 2-8: Near-surface geostrophic velocity and relative vorticity fields (10^{-6} s^{-1}) during March 1997 (a) and April 1998 (b). Red and black arrows indicate geostrophic velocity and the near-surface 5-day averaged, 40-hour low pass currents from the moorings. Colored areas present relative vorticity. (Hamilton and Lee, 2005).

Complex eddy circulation is found to dominate over the slope of the De Soto Canyon region, which is intensely affected by northward penetration of the Loop Current. This eddy circulation provides an effective mechanism by which to exchange material and heat between the shallow and deep waters as well as between the DeSoto Canyon region and the surrounding areas (Hamilton and Lee, 2005). Based on hydrographic surveys during March 1997–April 1999, Hamilton and Lee (2005) found that eastward flows prevail along the upper slope, south of Mobile Bay in five of seven surveys (Fig. 2-8a). During these surveys, there were anticyclonic eddies associated with the Loop Current over the deep waters pairing with ambient cyclonic

eddies to enhance cross-slope flows. One survey showed evidence that frontal cyclonic eddies of the Loop Current reach the upper and middle slope and cause a westward surface flow offshore of Mobile Bay. Again, these frontal eddies probably accompany other anticyclonic eddies to generate strong onshore jets (Fig. 2-8b).

2.2 Winds in the Northeastern Gulf of Mexico

Climate in the Gulf of Mexico is primarily determined by different air masses. Muller (1977) and Muller and Willis (1983) analyzed daily weather data in 30 years from a National Weather Service station in New Orleans, Louisiana, and identified eight major synoptic weather patterns, including Pacific High, Continental High, Front Overrunning, Coastal Return, Gulf Return, Frontal Gulf Return, Gulf High, and Gulf Tropical Disturbance. From these studies, Yocke et al. (2000) distinguished ten key synoptic weather types for the northeastern Gulf of Mexico, comprised of Midwest Continental High, Eastern Continental High, Bermuda High, Midwest Low, Gulf Front or Trough North/South, Gulf Front or Trough East/West, East Coast Low, Gulf High, No Gradient, and Hurricanes/Tropical Storms/ Depression, each of which is dominant in different seasons. Eastern Continent High and Midwest Low predominate in winter, Bermuda High and Midwest Continental High in spring and summer, Gulf Front and Trough North/South in spring, Gulf Front and Trough East/West in fall, Gulf High and No Gradient in summer and fall, and Hurricanes/Tropical Storms/Depression in fall (ibid.).

Accordingly, wind patterns are clearly different during different seasons. Winds are dominantly northerly and northeasterly in winter, and easterly and southeasterly in summer, and are also fairly spatially uniform in the eastern Gulf. In the transition seasons of spring and fall, winds are highly variable because of the presence of several synoptic features. For instance, northerly or northwesterly and southeasterly winds can occur in spring and summer due to the Midwest Continental High and Bermuda High, respectively; the Gulf Front and Trough North/South can result in northwesterly winds on the western part of the front and southeasterly winds on the eastern part in spring; otherwise Gulf Front and Trough East/West can lead to the northerly winds to the north of the front and the southerly winds to the south of the front. Monthly averaged winds are calculated for the period of 2005–2008 based on Climate Forecast System Reanalysis (CFSR) 1-hourly wind data.

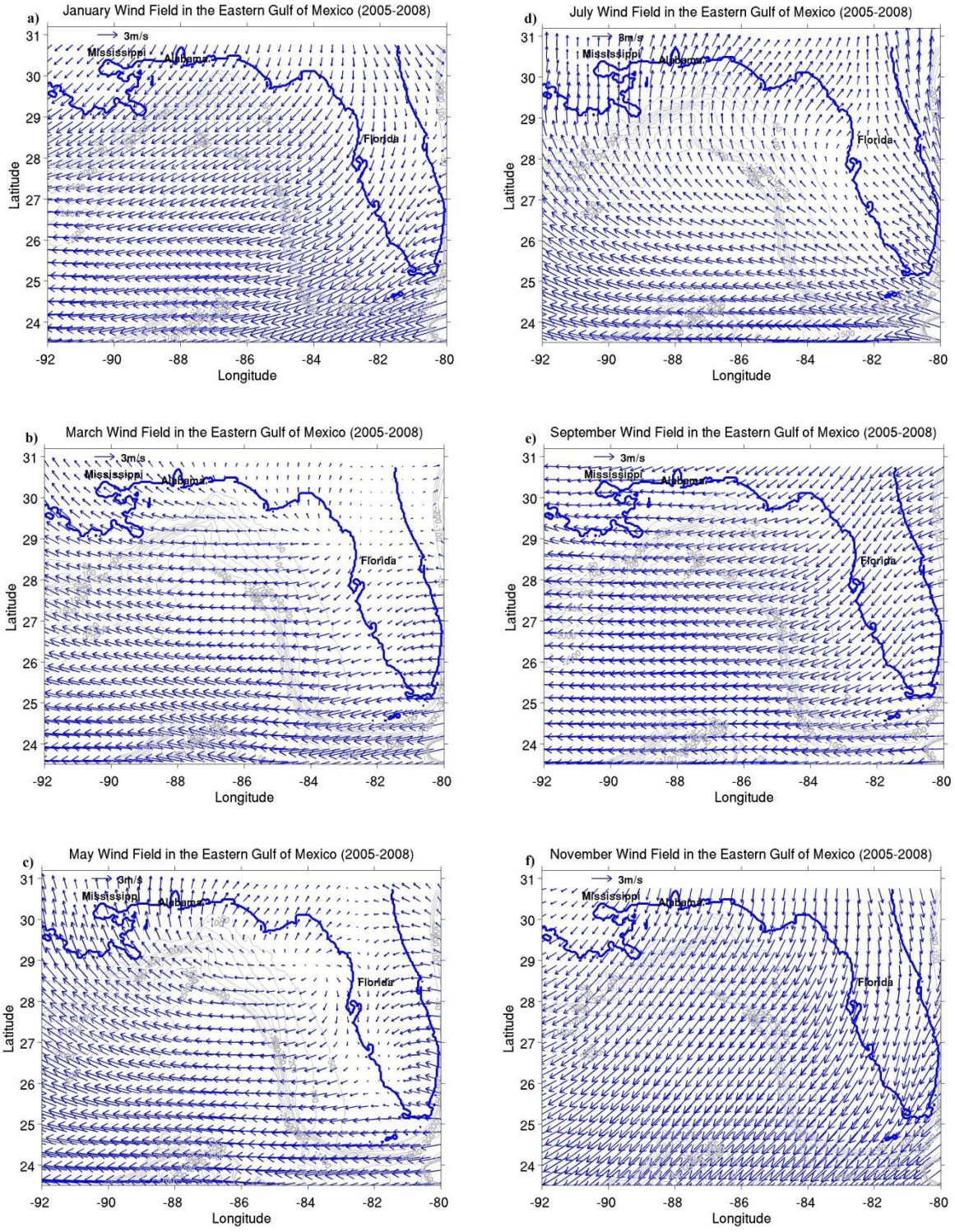

Figure 2-9: Monthly wind field in the eastern Gulf of Mexico.

These show that both magnitude and direction of winds change seasonally. Averaged winds have a large magnitude in winter and spring and are more persistent in winter and summer than in spring and fall (Figs. 2-9a to f). Wind directions are seen to shift more southerly and easterly in June and September, respectively. In fall, winds are relatively strong in September and October, which may be due to hurricanes in the study area during 2005–2008. In spring, the average direction of the winds tends to be more westward over the deep waters south of 29 ºN and more northwestward close to the coast (Figs. 2-9b and c).

2.3 DeSoto Canyon Region

The Gulf of Mexico was formed by separation of the mega-continent Pangea which began approximately 180 million years ago and subsequent movement of the Yucatan and the Florida Straits Blocks (Hine et al., 2013). Seawater came through the Mexican terrain from the Pacific Ocean, developing the Gulf of Mexico basin. The study area is located in the northeastern Gulf of Mexico and focuses on a prominent feature, the DeSoto Canyon. The deeper portion of the canyon was created by salt deposition in the western end of the South Georgia Rift Basin (ibid.). The DeSoto Canyon has a width of 120 km at 100 m water depth and separates two wide continental shelves and the slopes of Alabama and the Florida Panhandle. The canyon is a deep geomorphic embayment or part of the trench separating the west and north Florida shelves and functions as a transition between the continental and ocean sedimentary regimes. A series of smaller channel-like and canyon-like features lie within the DeSoto Canyon with a depth of 100 m or less (ibid.).

The study region is irregularly complex and spans from 27.5 to 31 ºN latitude and from 84 to 91 ºW longitude (Fig. 2-10). Its geometry changes greatly with isobaths converging from west Florida to the canyon and then widening in the Mississippi Bight. The width of the continental shelf varies considerably over the domain with the narrowest shelf area at the 200-m canyon isobaths and approximately 72 km away from the coast. The region is of particular economic and ecological interest with the largest coastal wetlands in the United States, where marine and terrestrial species such as birds, fishes and plants (Ko et al., 2004) are living. A diverse variety of economic activities is associated with the wetlands including fisheries, ecotourism and hunting. These greatly contribute to local and regional economics. Approximately 81 % of the total commercial fishing in the Gulf of Mexico and 40 % of the market value come from Louisiana; recreational fishing produces about $944 million annually (Raynie and Beasley, 2000; Day et al.,

2004). In addition, growth of oil and gas industries has been increasing in both the Gulf and the region, especially in recent decades when technological innovations in geophysical exploration, drilling and marine construction have been dramatically advanced. Offshore drilling rigs are concentrated in the northern Gulf of Mexico. Ninety seven percent of the offshore gas is produced off Louisiana and Texas, and seventy six percent of the offshore oil is from Louisiana (ibid.). Moreover, the Mississippi delta has one of the most extensive exploitations of gas and oil in coastal zones in the world. As a result, Louisiana is the second most important state in the petroleum industry which had more than 500 oil and gas platforms by 1990 and an accumulated revenue of $12 billion during 1926–1983 from coastal zones (ibid.).

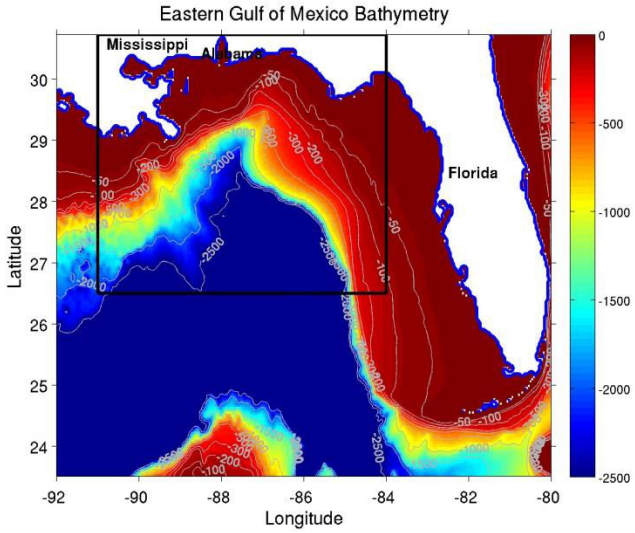

Figure 2-10: Bathymetry of the eastern Gulf of Mexico. The DeSoto Canyon area is outlined with the black box.

2.4 Upwelling and Downwelling

2.4.1 General Upwelling and Downwelling

Smith (1968) defined ocean upwelling as the ascending motion of water from subsurface layers because of horizontal surface divergence and subsurface convergence. Another definition of upwelling by Yoshida and Mao (1957) is given as “upward penetration of a mass of water into a surface mixed layer” and specifically coastal upwelling is “the rise of the thermocline toward the coast”. Downwelling is referred to as the descending of warmer water from the upper layers.

Based on spatial occurrence, ocean upwelling and downwelling can be classified into three types: equatorial, coastal and open-ocean upwelling and downwelling (Pond and Pickard, 1983). Coastal upwelling and downwelling can be caused by several factors, but mostly wind fields through the surface Ekman transport. It occurs, for example, along the California and Peru coasts, the Somalia coast, the northwestern and southwestern points of Africa. Classical Ekman theory shows that a steady wind blowing along the coast can produce surface currents 45º to the right (left) of the wind in the northern (southern) hemisphere. Because of friction between water layers, currents gradually veer to the right (left) when going deeper in the northern (southern) hemisphere. As a consequence, the Ekman spiral is generated in a few hundred meters of the ocean upper layers. In the northern hemisphere, the net mass transport in the surface Ekman layer is perpendicular and to the right of wind stress. This means that upcoast winds (with the coast to the left in the northern hemisphere) are generally responsible for offshore surface Ekman transport (Fig. 2-11). Surface horizontal divergence takes place in the near-shore zone and a cross-shore pressure gradient and associated geostrophic current trigger an onshore bottom Ekman transport. Therefore, subsurface waters are upwelled to compensate for this divergence. Conversely, downcoast winds (with the coast to the right in the northern hemisphere) account for downward movement of surface waters because the onshore surface Ekman transport builds up waters in the near-shore zone (Fig. 2-12).

Open-ocean upwelling can be caused by wind stress curl and eddy circulation. Counter-clockwise winds or positive wind stress curl attributed to hurricanes, storms and depressions produce surface Ekman transport away from the center and thus the thermocline is lifted up in the northern hemisphere. Cyclonic and anticyclonic eddies associated with upward and downward thermocline displacements, respectively, and their translation can give rise to upwelling and downwelling underneath the eddy path. Upwelling and downwelling have a wide range of time and length scales, primarily depending on driving forces. The wind has a synoptic scale and can be steady in some regions; correspondingly, wind-driven upwelling and downwelling tend to be persistent lasting a few days to a week and is seen approximately 30 km from the coast. The time scale of upwelling and downwelling set up is approximately one inertial period and upwelled water comes from below the Ekman layer, from typically about 50 to 200 m deep. Storm-induced vertical motions occur in both shallow and deep waters on time scales related to translation speed of the storm system. Oceanic eddies have diameters on the order of

tens to hundreds of kilometers and may be persistent over a period of several months or transient lasting a few hours. Furthermore, a propagating disturbance such as Rossby waves can make the thermocline move up and down over longer time and larger length scales.

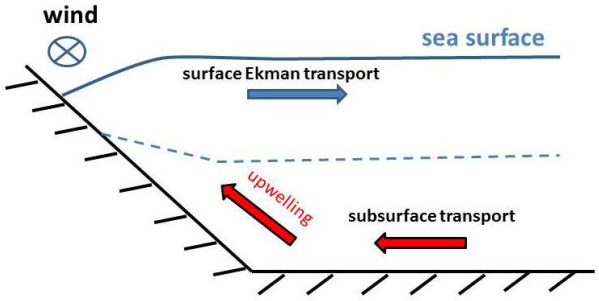

Figure 2-11: Coastal wind-driven upwelling.

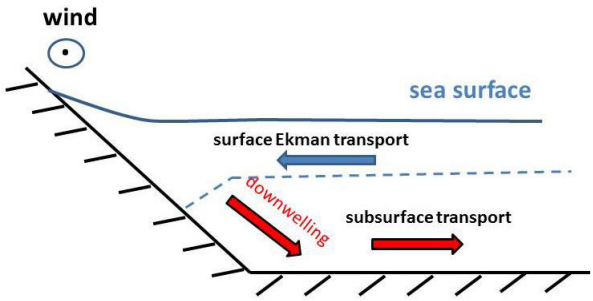

Figure 2-12: Coastal wind-driven downwelling.

Upwelling is a crucial process in the ocean and has been of particular interest to oceanographers since the 1960s. Most of the early studies were based on in situ observations which promoted understanding of both physical and biological aspects of upwelling on the continental shelf, for example, the Coastal Upwelling Experiment off the Oregon coast in 1972, the Coastal Upwelling Ecosystem Analysis program during 1972–1977, MESCAL I and II off the Mexico coast in the period 1972–1973, the JOINT I for the northwestern African coast in 1974 and the JOINT II for the Peruvian coast in 1977. Later on, the development of remote sensing technology advanced upwelling research programs, in particular in the open-ocean and inaccessible regions. Satellite and plane sensors allow continuous and effective collections of a wide range of observations and overcome disadvantages of traditional in situ and ship-based methods. Upwelling systems usually have a low sea surface temperature (SST), high chlorophyll concentration, lower SSH and specific patterns of the wind such as alongshore or positive wind stress, all of which are readily measured by remote sensing instruments with different spectral bands. For example, the visible band for chlorophyll, the thermal infrared band for SST, the passive microwave band for SST and sea surface salinity (SSS) and the active microwave band for SSH and sea surface roughness.

The earliest studies of coastal and shelf dynamics were mostly carried out for areas with relatively simple topography. Dynamics in regions with complex topographic features such as

submarine canyons and trenches remain an open question for oceanographers. Canyons are typically 10–15 km wide, 100–500 m deep, and about 45º steep (Kämpf, 2007) and have a unique circulation. Effects of submarine canyons were first observed off of Vancouver Island in the studies of Freeland and Denman (1982) and Klinck (1996). Abrupt changes in topography of the submarine canyons modify the relative vorticity and planetary vorticity and produce anticyclonic and cyclonic eddies. These account for generation of downwelling and upwelling processes as well as cross-shore exchange between the continental shelves and the deep ocean (Holton, 1992; Hickey, 1997). Upwelling in canyons is found to have a stronger flux than over the adjacent continental shelf and slope (Hickey, 1997; Kämpf, 2007).

Numerical analysis began in the 1940s and became a powerful tool to simulate vertical circulation in the oceans. Numerical experiments have been rapidly developed over irregular bathymetry since the 1990s. Allen (1996) used a linear theory of wind-induced flow over a very thin and finite length canyon to simulate numerically and analytically initial growing and steady state phases, and the results indicated that up-canyon flow appears 10 times greater than the cross-shelf break flow for a homogeneous fluid. Moreover, this study emphasized the role of water stratification in intensifying the up-canyon flow on orders of 50 times or greater. A semi-spectral primitive equation model (SPEM) built by Haidvogel et al. (1991) with coordinate transformation is useful for investigating circulation over irregular bathymetry at regional and basin scales. Klinck (1996) applied the SPEM 3.0 with periodic alongshore boundaries to a smooth canyon for weakly and strongly stratified flow. The influence of the canyon is determined by the direction of the alongshore flow; when this flow is to the right of the canyon, an upwelling takes place and creates strong cross-shelf transports. Results obtained by both Allen (1996) and Klinck (1996), which included a cyclonic eddy within the canyon, agree with observations to some extent, yet these studies did not account for a mean cyclonic pattern (She and Klinck, 2000). Another numerical experiment with the Rutgers University Regional Ocean Modeling (ROMS) by She and Klinck (2000) was also set up for a narrow canyon. A three-dimensional picture of circulation was achieved with wind forcing and stratification. The model indicated that upwelling winds produce onshore flow over and upstream of the canyon, and offshore flow downstream of the canyon in the upper layer of 100 m, resulting in the formation of a closed cyclonic ring. Flow inside the canyon is shoreward at 100–200 m (close to the canyon rim) and follows isobaths in the deeper layer. In addition, several different models and laboratory

experiments have been employed to quantitatively estimate mass fluxes over a shelf-break canyon. Examples include the Spectral Element Ocean Model (SEOM) by Haidvogel (2004), the COupled Hydrodynamical Ecological model for REgioNal Shelf seas (COHERENS) by Kämpf (2007), and a series of lab experiments by Boyer et al. (2004) and Mirshak and Allen (2005). Nonetheless, these studies mainly carried out laboratory and numerical experiments over idealized topography of the canyon region and suggested flow patterns within the canyons with different sizes and stratification conditions. They emphasized on the canyon itself which is relatively typical with the radius of the isobath curvature on the order of the deformation radius, and have not considered the large region covering submarine canyon and other driving forces rather than the wind on cross-slope canyon flows yet.

2.4.2 Upwelling and Downwelling in the DeSoto Canyon Region

Upwelling has been observed in the DeSoto Canyon region. A well-documented example is the anomalous persistent upwelling event during summer and spring 1998, which caused dense algal blooms and mass mortalities of fishes and invertebrates on reefs 20 km east of Panama City in May, reefs west of Destin in June–mid July, St. Andrew Bay, Pensacola Gulf Shores and Alabama in July (Collard and Lugo-Fernandez, 1999; Collard et al., 2000). Marine organisms had low-dissolved-oxygen symptoms; sluggish fishes were seen below the strong thermocline. Demersal organisms such as rock shrimps and crabs came to the surface at St. Andrew Bay. Dead fishes were reported to be floating at the surface offshore for the period of 10 weeks and at Panama City beach during late June–mid July. AVHRR SST products indicated 3 to 6 °C lower temperature than normal and high chlorophyll concentration appeared in SeaWiFS images off the Florida Panhandle in the period May–July 1998 (Muller-Karger et al., 2000). Some efforts were made to identify the main causes for this upwelling event as well as mass mortality of marine organisms. Collard and Lugo-Fernandez (1999) reported unusual climatic conditions in the northeastern Gulf of Mexico associated with an El Nino event in summer 1998 provided anomalous wind patterns with a dominant eastward alongshore wind component or upwelling-favorable winds in May through June. Nowlin et al. (2000) and Muller-Karger et al. (2000) found that cooling SST events followed the eastward alongshore winds by examining time series of SST and alongshore winds at Coastal-Marine Automated Network meteorological station on Dauphin Island (DPIA1) (Fig. 2-13). It is noticeable that cyclonic and anticyclonic eddies were

observed in this area (Fig. 2-14). Eastward current attributed to an anticyclonic eddy at the DeSoto Canyon can generate the onshore bottom Ekman transport and then upwelling in the shallow water (ibid.). Weisberg and He (2003) discussed the remote impact of the Loop Current on the northeastern Gulf in 1998; as a consequence, the strong eastward current elevated the isopycnals along the shelf slope, providing preconditions for cold waters to upwell onto the shelf by local winds.

Furthermore, earlier observations show that the west Florida shelf sea level variations and flow patterns are strongly correlated with wind stress (Koblinksky and Niiler, 1980; Mitchum and Sturges, 1982; Marmorino, 1983 and Mitchum and Clarke, 1986). The west Florida shelf flow patterns were examined in response to upwelling-favorable offshore and alongshore wind stresses in Li and Weisberg (1999), using a three-dimensional Princeton Ocean Model (POM) simulation. Uniform northwesterly wind stresses can generate a broad coastal southeastward jet along the Florida Panhandle, and subsequently the associated onshore bottom Ekman transport sets intense and extensive upwelling near Apalachicola Bay. Because of the partial closure of the shelf at the Florida Keys, a return flow is northwestward just along the shelf break and an associated cross-isobath disturbance may propagate topographic Rossby waves, which can reach the DeSoto Canyon. On the other hand, uniform offshore or northeasterly wind stresses provide more complicated circulation; northwestward and southwestward flows occur north and south of the west Florida shelf, respectively and the upwelling tends to establish over the shelf from the Florida Panhandle to south of the west Florida shelf (ibid.). Using the same POM model, Yang and Weisberg (1999) examined the climatological response of the west Florida shelf to wind forcing and demonstrated that low coastal sea level related to offshore surface transport occurs along the Florida Panhandle to the Florida Keys in the period of October to March, otherwise fairly high sea level likely happens in the period of April to September.

Also, Cragg et al. (1983) analyzed sea level observations from Pensacola, Cedar Key and St. Petersburg during 1965–1967 and inferred that the maximum sea level response is for alongshore winds with a response of 60 cm for 1 dyn/cm^2 alongshore wind stress and a lag time falls from 10 to 24 hours. An extended study from Marmorino (1982) examined hourly sea level at 12 stations from Pensacola to Key West and atmospheric data at 5 stations for the period 1 January–30 April 1978 and noticed the sea level response propagates faster in the same direction with southeastward alongshore wind stress attributed to cold fronts. Sea levels are found to lag the

wind by about 18 hours in the DeSoto Canyon region. Moreover, to reproduce spatial variability with spatially uniform winds, the author employed a linear two-dimensional model to realistic bathymetry and coastline from Panama City to Key West, illustrating coastally trapped signals on a scale of about 60 km as the arrested topographic waves from Csanady (1978). A linearized two-dimensional storm-surge model with realistic bathymetry and coastline from New Orleans to Key West was conducted by Hsueh et al. (1982) to assess the influence of a cold front passage on sea level fluctuations. A drop in shelf sea levels is observed in the cold front period of about 6 days and afterwards a wave-like motion propagating toward the north is accountable for alongshore velocities unassociated with local winds (ibid.). The northerly wind bursts in winter are considered in accounting for establishment of continental shelf waves at the Florida Keys, which can pass the west Florida shelf in the counter-clockwise direction and generate robust coastal currents in the DeSoto Canyon region as well as within the canyon (Hsueh and Golubev, 2002). The onshore bottom Ekman transport associated with these strong currents around the canyon can combine with upslope flows within the canyon due to the northerly wind pile up so that a strong upwelling is generated over the canyon's head.

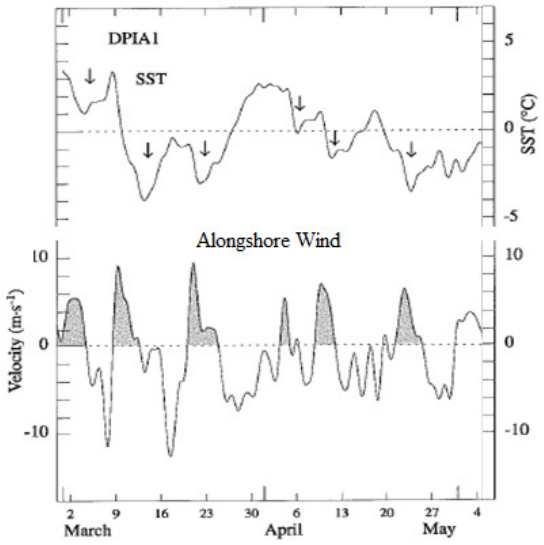

Figure 2-13: Sea surface temperature (upper) and alongshore wind component of 10 m wind (lower) observed at Coastal-Marine Automated Network meteorological station on Dauphin Island (DPIA1) in the period of March–May 1998. These time series were 40-hour low-pass filtered and the seasonal warming trend was removed from the sea surface temperature record by a cubic fit. Shaded winds indicate upwelling favorable alongshore component and positive SST means warming events. (Nowlin et al., 2000).

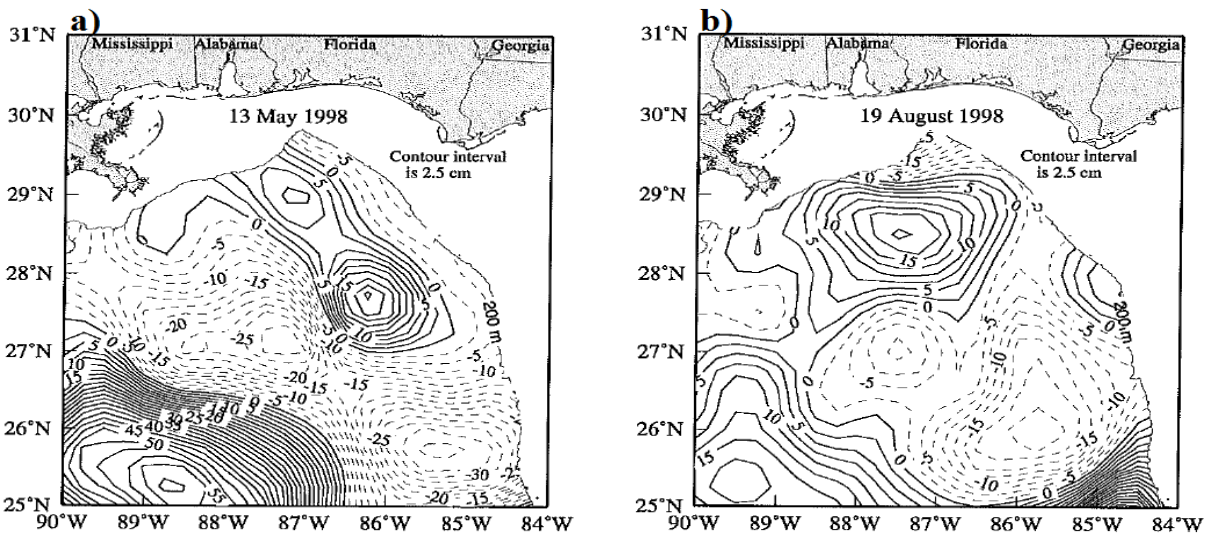

Figure 2-14: Snapshots of sea surface height anomaly from TOPEX/POSEIDON and ERS-2 altimeter data on 13 May 1998 (a) and on 19 August 1998 (b). Solid and dashed contours indicate positive and negative SSH anomaly. (Nowlin et al., 2000).

CHAPTER 3

HYPOTHESES: POSSIBLE MECHANISMS OF CROSS-SLOPE FLOW IN THE DESOTO CANYON REGION

Two mechanisms that drive cross-slope flows or upwelling and downwelling in the DeSoto Canyon region are considered in this study. First, the local wind is considered, as it is the major cause of upwelling and downwelling along the continental margins and in the upper layers of the ocean. This kind of upwelling and downwelling exhibits inherent synoptic scales on the order of days temporally and tens to hundreds of kilometers spatially. Second, remote processes related to the Loop Current are considered. These processes have a long time scale, on the order of weeks to months, and a large horizontal scale, on the order of hundreds to thousands of kilometers. Cross-slope flows or upwelling and downwelling over the continental slopes may result from either of these two mechanisms. The persistent upwelling event in 1998 was a result of a combination of these mechanisms.

3.1 Wind-driven Upwelling and Downwelling

Wind-induced upwelling and downwelling are relatively persistent lasting for several days over a large spatial scale. This is particularly the case, during winter and spring when wind fields are greater because of the passage of strong cold fronts and winter storms in the northeastern Gulf of Mexico. According to Moeller et al. (1993), approximately 30 to 40 cold fronts influence the Louisiana coast between October and April. Associated northerly winds can produce a large drop in sea level close to the coast, causing a cross-shelf pressure gradient. A barotropic alongshore flow can be established which is in geostropic balance and accounts for onshore bottom Ekman transport and coastal upwelling. On the other hand, during summer southeasterly winds prevail in the northeastern Gulf and northwestward flows dominate over the west Florida shelf, resulting in onshore surface Ekman transport and hence a region of downwelling (Yang and Weisberg, 1999). In addition, downwelling can take place over the middle and outer shelf of the Florida Panhandle in winter, when the northeasterly winds generate an offshore flow at the near-bottom depths (ibid.).

Vertical disturbances due to the Ekman transport can propagate as coastally trapped waves. This means that the strength of coastal upwelling and downwelling in a specific region relies on the combined effect of local forcing and incoming wave-like disturbances that originate far away

(Walin, 1972; Gill and Clarke, 1974; and Maksimova and Clarke, 2013). According several earlier studies by Gill and Schumann (1974), Clarke (1977) and Mitchum and Clarke (1986), the synoptic-scale winds drive a low-frequency sea level elevation along the west Florida shelf. The low-frequency sea level response to the winds can be characterized by a succession of large-scale wave-like motions. A forced, first-order wave travels along the shelf from north to south with the wind and subsequently a free wave develops at the southern end of the west Florida shelf (Key West). This free-propagating wave has opposite direction to the winds and has a phase speed of approximately several hundred kilometers per day. In winter, cold front winds are generally uniform and have comparable time scale to upwelling and downwelling setup, therefore, after one to two days, free waves are formed along the west Florida shelf and modify coastal sea level and/or vertical motions along their path, including the DeSoto Canyon region (Fig. 3-1).

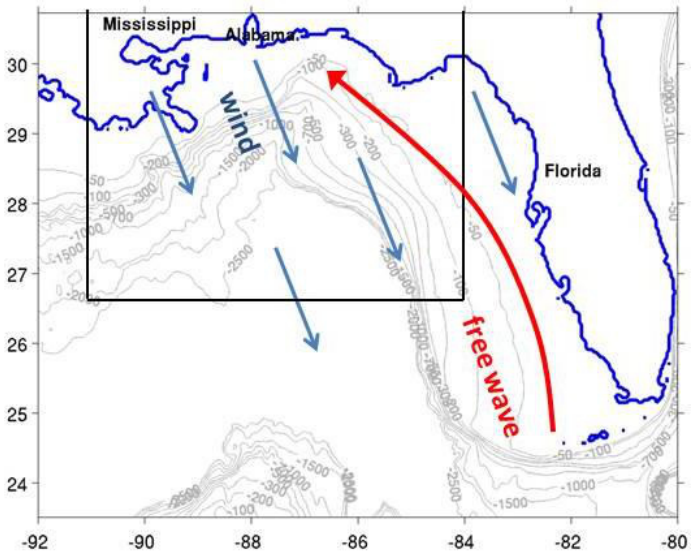

Figure 3-1: Low-frequency response on the west Florida shelf to the winds. Blue and red vectors present the wind and free wave, respectively. The DeSoto Canyon region is outlined with the black box.

3.2 Upwelling and Downwelling Induced by Mesoscale Oceanic Eddies

Ocean dynamics in the deeper part of the DeSoto Canyon region are impacted by both the Loop Current and mesoscale eddies. Observations show that the Loop Current reaches as far north as 27–27.5 °N approximately 10 % of the time and 28 °N about 5 % of the time during the

period of 1976–2003 (Vukovich, 2012). The 54-year GoM-HYCOM simulation shows that the occurrence probability of the Loop Current front at 27.5 °N is about 0.05 (Fig. 2-3). Peripheral cold-core cyclonic eddies are commonly observed along the boundary of the Loop Current. They move clockwise at speeds of 2 to 20 km per day and have length scales of order 100 to 250 km (Vukovich, 1986; Vukovich et al., 1979).

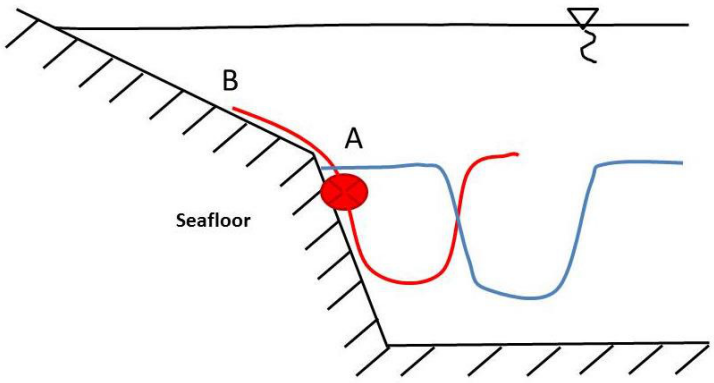

Figure 3-2: An anticyclone impinging upon the slope. Red and blue contours represent the thermocline underneath an anticyclone at the moments before and after approaching the slope, respectively. The associated current runs into the page. Points A and B show the position of the thermocline before and after anticyclone's impingement.

The Loop Current warm-core and cold-core eddies have a relatively high frequency zone over the slower Mississippi-Alabama slope; the high frequency zone is centered at around 27.5 °N and 89.5 °W for warm-core eddies (a maximum of 7 %) and at 27.5 °N and 88.5 °W for cold-core eddies (a maximum of 30 %) (Vukovich, 2007). In addition to raising and dropping the underlying thermocline, the eddies greatly contribute to the cross-slope flows when they come into contact with the continental slope. An anticyclone tends to be squeezed against the slope and uplift the thermocline onto the shelf (Fig. 3-2) (Tomczak, 1996). Cold and nutrient-rich waters can upwell on the outer shelf or upper slope. Dynamic uplift can also occur as strong currents flow along the right of the continental slope in the northern hemisphere. Conversely, a cyclonic eddy impinging upon the shelf or slope can generate a drop of the thermocline on its onshore fringe and, hence, warm water can travel further downslope. Therefore, the associated upwelling and downwelling have a wide range of time and length scales because of the diversity of the eddies.

3.3 Upwelling and Downwelling Remotely Induced by the Loop Current

The Loop Current is characterized by swift currents in the clockwise direction, warm temperatures and high sea surface height. It exhibits two phases: extended and retracted. In the extended phase, the Loop Current deeply penetrates into the Gulf of Mexico and sometimes reaches the DeSoto Canyon slope. Its high pressure deepens the isopycnals beneath but can uplift the isopycnals on its shoreward boundary or over the shelf break.

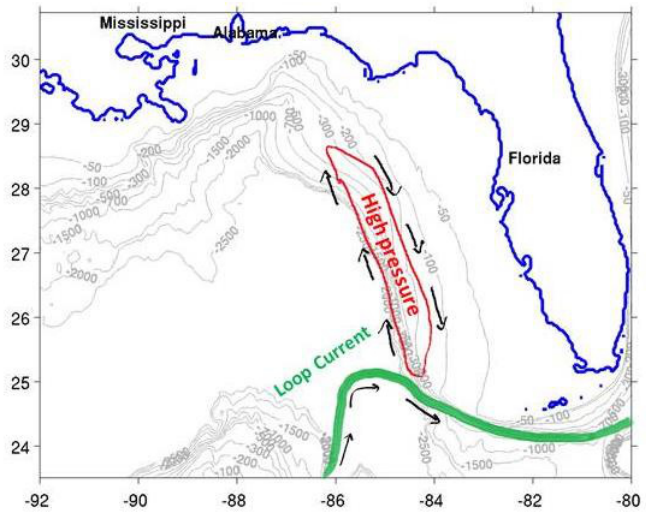

Figure 3-3: The Loop Current impinging upon the west Florida shelf. The green contour represents the Loop Current front; black arrows show currents; the red contour shows the high pressure area north of the impingement point; grey contours in the background are isobaths (-50, -100, -200, -300, -500, -700, -1000, -1500, -2000 and -2500 m). Horizontal and vertical axes indicate longitudes and latitudes.

In addition to the direct impact, the Loop Current is capable of providing a remote impact on the DeSoto Canyon cross-slope flow. When the Loop Current hits the west Florida shelf, a stagnant point develops, causing a local high pressure due to the Bernoulli principle. Otherwise, the Loop Current is squeezed south of the stagnant point by the presence of the west Florida shelf, establishing a pressure drop (Hetland, 1999). A drop in pressure occurs along the west Florida slope and can modify circulation along the west Florida slope. Also, a small portion of the Loop Curent splits off and a tongue of associated high pressure leaks along the west Florida slope and decays to the north (Fig. 3-3) (Shi and Nof, 1993; Hetland, 1999). Accordingly, there

is a northward flow west of the tongue and a southward flow along the shelf break east of the tongue.

In particular, when the Loop Current retracts to the south after shedding eddies, it can contact the west Florida shelf off the Florida Keys. Southward jets shoreward of the high pressure area can extend further onshore. An associated drop in pressure is located near the isobath convergence area, increasing the impact of the Loop Current on the shelf circulation along the west Florida shelf. Moreover, propagation of the high pressure related to the Loop Current along the slope can be described in the same way as the heat conduction along a rod, which is similar to arrested topographic wave theory (Csanady, 1978; Hetland, 1999).

CHAPTER 4

DATA AND METHODS

4.1 GoM-HYCOM Ouputs

Cross-slope flow in the DeSoto Canyon region is studied using hydrodynamic data from a 1/25° free-running multi-decadal numerical simulation using the Gulf of Mexico HYbrid Coordinate Ocean Model (HYCOM). The 1/25° regional HYCOM Gulf of Mexico domain (hereafter referred as GoM-HYCOM) is configured from 18.9 to 31.96 °N and from 98 to 76.4 °W (Fig. 4-1). The vertical grid uses 20 hybrid layers, which in the open ocean below the mixed layer, are mainly isopycnal layers. Model bathymetry is derived from the Naval Research Laboratory Digital Bathymetry Data Base 2-minute resolution (www.7320.nrlssc.navy.mil/DBDB2_www). Monthly climatology river inflow is simulated at 40 locations along the Gulf coast. The GoM-HYCOM has five open boundary conditions which are derived from a bi-weekly climatology produced by a free-running simulation of the 1/12° Atlantic HYCOM. The simulation was initialized from a 5-year spin-up run that started from rest and used the Generalized Digital Environmental Model 3.0 (GDEM) climatological fields and was forced with atmospheric fields from the Fleet Numerical Meteorology and Oceanography Center's Navy Operational Global Atmospheric Prediction System (NOGAPS) (Rosmond et al., 2002). Following spin-up, atmospheric forcing (10-m wind speed, wind stress vector, 2-m air temperature, 2-m atmospheric humidity, surface short-wave and long-wave heat fluxes and precipitation) is derived from hourly fields of the Climate Forecast System Reanalysis (CFSR) (Saha et al., 2010) in the period 1992 through 2009. This 18-year record of surface forcing is repeated three times to produce the continuous 54-year model integration. More details on the GoM-HYCOM and comparison between the Loop Current statistics from the GoM-HYCOM outputs and altimeter data can be found in Dukhovskoy et al. (2014) and at hycom.org/dataserver/goml0pt04.

HYCOM is an improved version of MICOM (Miami Isopycnal Coordinate Model) by Bleck et al. (1992) (HYCOM user's guide, 2003). In HYCOM, vertical coordinates are smoothly transitioned from isopycnals in the open and stratified ocean to terrain-following in shallow waters and to z-level in unstratified waters and the mixed ocean layer (Fig. 4-2). Thus, HYCOM

is suitable for simulating circulation in both the deep and shallow waters, which is of importance in regional and basin-wide studies. More details can be found in Chassignet et al. (2003; 2006).

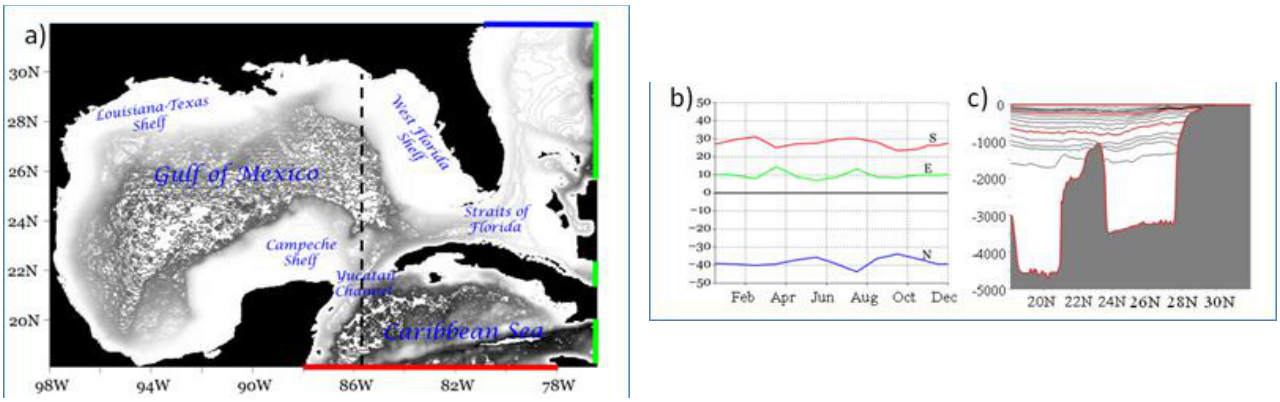

Figure 4-1: a) The Gulf of Mexico HYCOM model domain. The open boundaries shown with red, green and blue lines are set by the 1/12° Atlantic HYCOM. b) Volume fluxes (Sv) along the GOMl0.04 open boundaries are calculated from nesting climatology velocity fields derived from the 1/12° Atlantic HYCOM; positive values indicate fluxes coming into the domain; red, green and blue lines represent the vertically integrated fluxes at the open boundaries shown in panel a. c) Snapshot of hybrid vertical layers along the meridional cross-section (the dashed line in panel a); red contours are used to mark every 5th layer. (courtesy of D. Dukhovskoy).

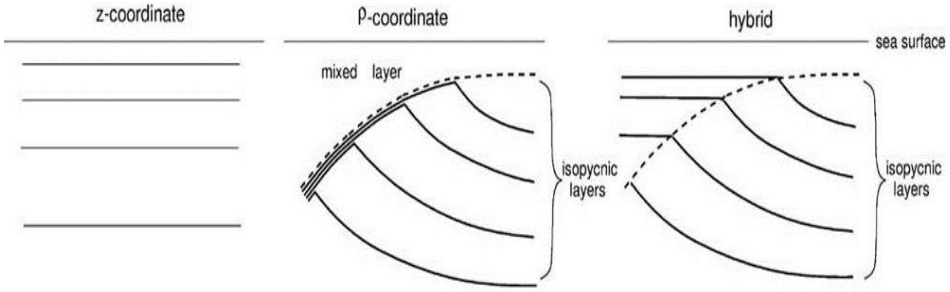

Figure 4-2: Vertical coordinate systems commonly used in ocean circulation models. (Chassignet et al., 2003).

4.2 Identification of Upwelling and Downwelling from Model Outputs

Upwelling and downwelling are often described in terms of its consequences (e.g., chlorophyll- rich, anomalously cold near-surface waters and nitrate (nutrient) concentration) or causes (alongshore wind stress and accompanying coastal sea level anomalies) that may be easily observed via satellites and in-situ measurements (Abbott et al., 1987; Abbott and Barksdale, 1991; Bakun, 1993; Walker et al., 2005; Zavala-Hidalgo et al., 2006; Garcia-Reyes et al., 2014).

Rarely is upwelling and downwelling described in terms of the actual vertical motion of the water, likely because this is a difficult quantity to measure due to its relative small size compared to the horizontal components. For this study, time series are constructed to describe upwelling and downwelling from the GoM-HYCOM simulation.

This study is primarily focused on upwelling and downwelling associated with near-bottom cross-slope flow. The vertical velocity near the seafloor may be defined from the horizontal velocity field as:

$$w_b = \vec{v}_b . grad(H)$$

where H is water depth and $\vec{v}_b$ is horizontal velocity field. At each model horizontal grid point in the region (at the depths down to 1000 m), a time series of w_b is estimated from the model data which has three-hourly output time in the period of 1998 and 2005 through 2008 and where $\vec{v}_b$ is taken as the horizontal velocity in the deepest active model layer at each horizontal location. The topography gradient is spatially smoothed over approximately 22 km. A positive value of vertical velocity indicates upwelling and a negative value indicates downwelling. Wind-driven upwelling over a shelf with complex bathymetry may deviate substantially from this simple view of coastal upwelling. The DeSoto Canyon study area has a complicated bathymetry, where the isobaths are oriented in the southeast-northwest direction in the eastern portion, abruptly change by nearly 90° at the DeSoto Canyon's head and become northeast-southwest in the western portion. As the assumptions inherent to the classical coastal upwelling depiction (uniform shelf width and uniform winds in relation to the coastline) may be not applicable, more complicated dynamics become important. The cross-shelf pressure gradient responsible for upwelling and downwelling will have alongshore variations that will propagate in a fashion resembling the arrested topographic wave (Csanady, 1978). Thus, the near-bottom cross-isobath flow will no longer entirely compensate for the cross-shelf surface Ekman transport driven by the local alongshore wind component. Fundamentally, this becomes a three-dimensional problem that may be tackled by integrating the wind stress along the dominant shelf wave mode propagation characteristic following Mitchum and Clarke (1986). If, however, the wind field is assumed to be nearly uniform over the shelf to the east of DeSoto Canyon over time scales comparable to the set-up time for upwelling and downwelling (order of 1 day), it is reasonable to analyze the cross-isobath bottom flow in relation to the local wind vector as is discussed below in Section 5.1.

The time series of w_b represents the vertical movement of water along the bottom slope. It may rapidly respond to changes in the horizontal circulation induced by winds, shelf waves, inertial oscillations and other high frequency events. Changes in isopycnal or isotherm depths that are often considered the primary indicator of upwelling and downwelling result from the time-integrated effects of the vertical velocity. This time integration effectively filters out the high-frequency fluctuations of vertical velocity and thus the resultant time series is useful for analyzing the low-frequency effects of upwelling and downwelling.

The upward/downward movement of isopycnals along the continental slope may be diagnosed readily by taking advantage of the HYCOM isopycnal coordinate. For deeper model layers, layer interfaces approximately follow the isopycnals. The movement of water up and down the slope at these depths is indicated by the movement of the intersection of layer interfaces with the model seafloor. For the GoM-HYCOM configuration used here, the 14th to 18th model layer interfaces have been identified as existing at depths corresponding to the continental slope in the DeSoto Canyon region (approximately from 250 to 1100 m) (Fig. 4-3). They are also deep enough so that they do not convert to geopotential or sigma coordinates during the model integration. These layer interfaces lie between model layers with target potential densities of 27.03, 27.22, 27.38, 27.52, 27.64 and 27.74 kg/m^3.

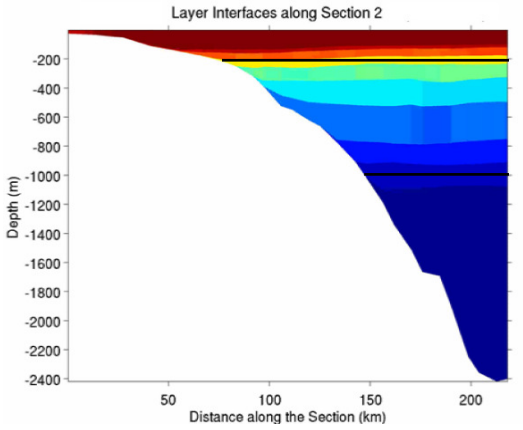

Figure 4-3: Model layer temperature, from which the layer interfaces may be seen, across a section (S2 in Figure 4-4). Black lines show the 250 m and 1100 m depths.

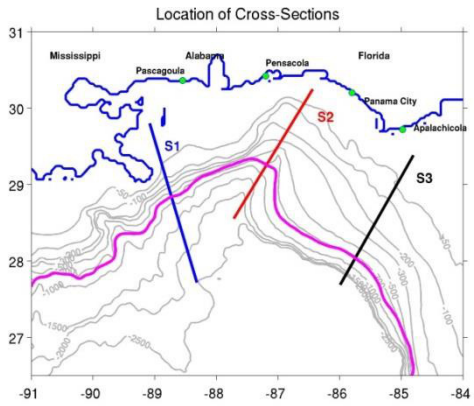

Figure 4-4: Location of three cross-sections S1 (blue), S2 (red) and S3 (black). The magenta contour indicates a specific layer interface.

The movement of the intersection of these interfaces with the ocean floor along three cross-sections in the domain (Fig. 4-4) is computed from the GoM-HYCOM data. The result is a set of time series of the locations of these interface/seafloor intersection points along the three cross-sections. Corresponding time series of the depths of these interface/seafloor intersections are also constructed, as the sections have been chosen such that the bathymetric depth along the sections is monotonic. The time series of an interface depth anomaly is obtained by subtracting the time-averaged depth of the interface from daily depth values over 36 years of the GoM-HYCOM simulation. These time series are used below in Section 5.2 to investigate the low-frequency upwelling and downwelling across the continental slope in the DeSoto Canyon region due to local and remote mesoscale circulation.

CHAPTER 5

RESULTS

This chapter focuses on results obtained from different diagnostic approaches to identifying upwelling and downwelling induced by cross-slope flows in the DeSoto Canyon region and other relevant mechanisms. Spatial variability of the near-bottom vertical velocity is calculated over the continental shelf and slope and its relation with local wind is determined. The results show a deviation of the wind-driven upwelling for this bathymetrically complex region from the classic theory that applies to a long straight coastline. In addition to the factors with high temporal frequency, the Loop Current and chaotic eddies directly and indirectly cause upwelling and downwelling over both the shelf slope and shelf break. Examples of the Loop Current's impact during the retracted and extended phases are provided. Further analysis of the Loop Current-induced pressure perturbation along the west Florida shelf to the DeSoto Canyon domain is presented and discussed in the context of the theories of Hetland (1999) and Weisberg and He (2003). Large-scale upwelling and downwelling are identified by analyzing vertical movement of the HYCOM layer interfaces at three representative cross-sections in the western part, over the canyon and in the eastern part of the study domain. A selection of characteristics of the upwelling and downwelling such as horizontal and vertical excursions and event duration are also included.

5.1 Wind-induced Upwelling and Downwelling

A correlation analysis is used to determine the relationship between cross-isobath flow, given by the time series of w_b defined in Section 4.2, and along-isobath wind component. A time series of three-hourly winds is derived from the CFSR 1-hourly winds data and then projected on the local isobath vector. These projected values are calculated for 1998 and 2005 through 2008. Three-hourly vertical velocities are calculated from three-hourly bottom horizontal velocities for the corresponding period. Correlation coefficients are estimated at each horizontal model grid point over the continental shelf and slope (Fig. 5-1). Strong correlation is restricted to the shallow waters in agreement with earlier studies (Mitchum and Sturges, 1982; Weisberg and He, 2003). Regions of relatively high correlation extend further offshore on the eastern shelf than on the western shelf; coefficient magnitudes of 0.3 to 0.4 are seen out to 200–300 m water depths

from southeast of Apalachicola to east of Pensacola. There is a zone of stronger correlation (near 0.65) located on the inner and middle Alabama shelf. In contrast, areas of poor correlation (< 0.25) lies over the outer Alabama shelf, along the western rim of the DeSoto Canyon and over the shelf regions near Pensacola, the Mississippi delta, Cape San Blas and Apalachicola, where the isobath curvature is most pronounced.

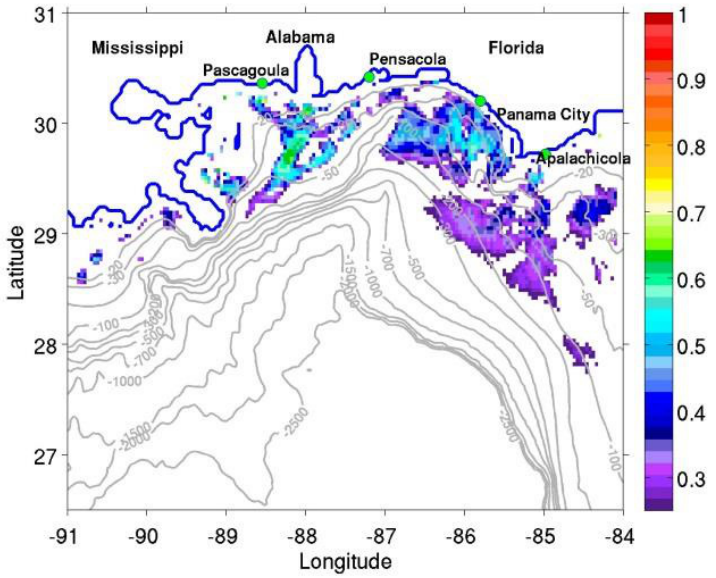

Figure 5-1: Map of correlation coefficients between along-isobath wind components and near-bottom cross-slope velocities. Gray contours in the background are the isobaths. The blue line is the coastline. Coefficients less than 0.25 are not shown.

The DeSoto Canyon isobaths are not straight, thus, it is not clear how to define the "along-isobath" orientation on which to project the local wind vector for this analysis. By varying this projection vector, one can determine the wind direction that is most related to the cross-isobath near-bottom velocity variability, and thus the wind direction that is most upwelling-favorable. This better determines how strongly related the upwelling and downwelling are to the local winds. The local wind vector is projected onto a vector that is rotated through different angles, varying between +90° and -90° around the local isobath vector. For each angle, the correlation is computed between this projected wind component time series and the vertical velocity time series. The maximum correlation coefficient at a given point over all angles is then determined (Fig. 5-2). The correlation coefficients are substantially increased, with larger areas of relatively

high correlation, compared to the results of the calculation using the along-isobath wind component. It is now apparent that the local winds are more strongly correlated with the near-bottom cross-slope velocities near the Mississippi delta and around Cape San Blas and Apalachicola. Higher correlation coefficients of 0.65 to 0.8 are found on the inner shelf and 0.5 to 0.6 on the middle shelf. Correlation tends to reduce with increasing water depth, with coefficients of 0.4 to 0.5 on the outer shelf and around 0.3 beyond the shelf. In the west of the domain, significant correlation is limited to the shallow waters up to 50 m. However, to the east and over the canyon's head, the significant correlation expands offshore to 300 m depth. There are still poor correlation zones located along the western rim of the canyon, from 50 to 200 m depths off Pensacola as well as the outer shelf off the Mississippi delta. It is worth noting that the influence of the local winds in the east of the domain can be stretched out further over the canyon and to the east from Pensacola.

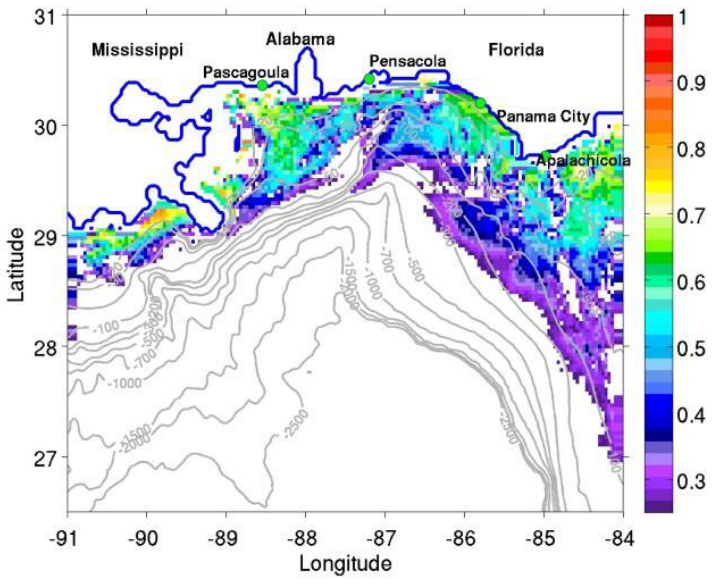

Figure 5-2: Best correlation coefficients between winds projected onto any azimuth and near-bottom cross-slope velocities. Gray contours in the background are the isobaths. The blue line is the coastline. Coefficients less than 0.25 are not shown.

The angle of the vector onto which the wind vector is projected that yields the highest correlation is computed for each model point of the DeSoto Canyon region. This "best" angle predominantly ranges from 80 to 160° (clockwise from the north) (Fig. 5-3) or from a southwest-

northeast to northwest-southeast orientation. The angle increases from east to west or turn clockwise by approximately 80 to 120° east of Apalachicola to Destin and 140 to 160° west of the canyon. A few areas in the Mississippi Bight, off Cape San Blas and Apalachicola Bay have the "best" angle being greater than 250°. One possibility is that the Ekman layer may not completely develop in these shallow areas (depths of about 20 to 30 m), which affects the values as the Ekman transport is integrated over a shallower layer. Furthermore, these areas are close to the river mouths such as the Mississippi River and Apalachicola River and therefore another possibility is that strong stratification due to river output provides a counter effect to the evolution of the Ekman layer. Generally, the preferred projection angles are profoundly different from most of the DeSoto Canyon continental shelf.

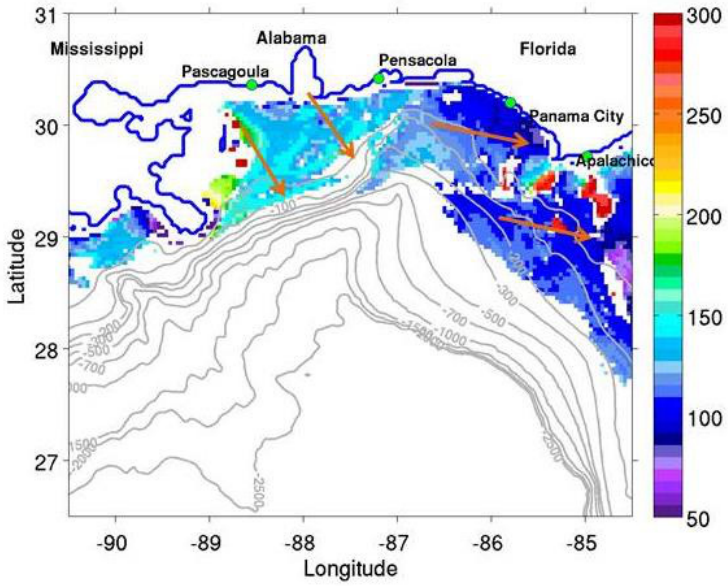

Figure 5-3: Best projection axis angle (θ) of winds in degrees (clockwise from the north). Gray contours in the background are the isobaths. The blue line is the coastline. Orange arrows indicate orientation of the preferred vector. Angles for regions with correlation coefficients less than 0.25 are not shown.

If the DeSoto Canyon region were a shelf with simple geometry conforming to the simple coastal upwelling model, the "best" angle would be oriented parallel to isobaths. But as discussed above, curvature of the shelf means that the wind-forced cross-shelf pressure gradient propagating along the shelf causes a deviation in the wind angle that is most related to local

cross-slope near-bottom flow. The preferred angle of the wind is distinctly different from the local isobath orientations particularly to the west of the canyon and to the east of Apalachicola, whereas the difference is small on the eastern shelf (Fig. 5-4). The preferred wind angle appears to be rotated about 40 to 90° and 20 to 40° clockwise of the local isobath orientation in the Mississippi Bight and on the Alabama shelf, respectively. There is a slight difference in angle, about ± 20° on the inner and middle shelf from Cape San Blas to Panama City, off Alabama and on the outer shelf from the canyon to the east. It implies that along-isobath winds drive the upwelling east of the canyon.

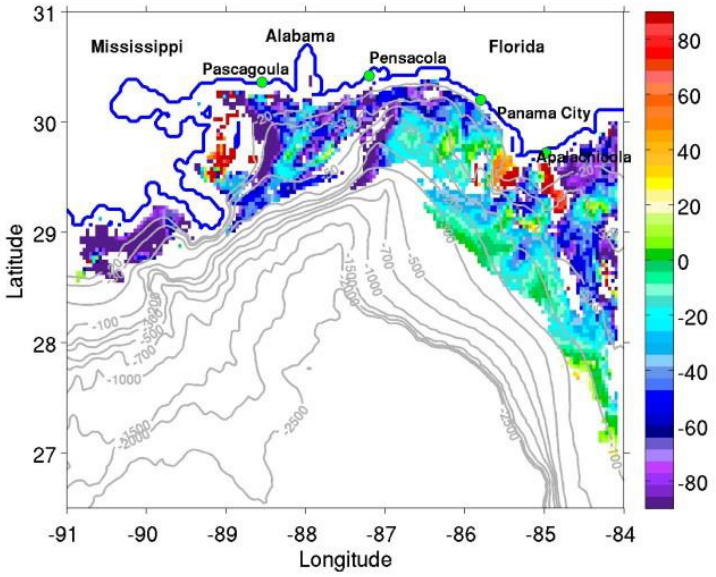

Figure 5-4: Difference in angle (°) between "best" projected vector of winds and local isobath vector. Gray contours in the background are the isobaths. The blue line is the coastline. Angles for regions with correlation coefficients less than 0.25 are not shown.

The predominant "best" orientation is southeast-northwest. It implies that the northwesterly wind is favorable for coastal upwelling over much of the region. Fernandez-Partagas and Mooers (1975) and Li and Weisberg (1999) show that this wind is predominantly associated with winter cold fronts as well as upwelling-favorable conditions along the west Florida shelf through Key West. The wind field over the west Florida shelf in the winter is influenced by a series of cold fronts propagating to the south that can cause a low-frequency response. This response can be described by southward-propagating waves forced on the west Florida shelf and associated free

waves originating at Key West. The non-locally generated free waves provide an explanation for the large departures in angle which occur downwave from strong bends of the isobaths at the DeSoto Canyon and at Cape San Blas despite the strong correlation of the winds and vertical velocity. Lag time between the winds and upward/downward motions is an important factor due to the influence of the time scales of wind-driven upwelling and downwelling setup and wind-induced propagation. The "best" lag time with the preferred projection winds is estimated to be less than 12 hours.

5.2 Cross-slope Flow Induced by Mesoscale Circulation

To investigate the cross-slope flow, the time series of the depths of interface/seafloor intersections along three representative cross-sections discussed in Section 4.2 are analyzed. The depth of the intersection between an interface and a section is determined over 36 years and is referred to as depth of the interface hereafter.

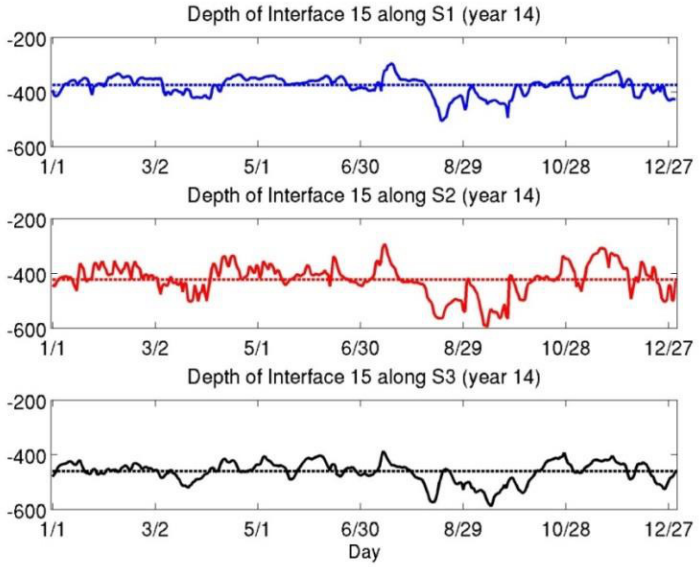

Figure 5-5: The time series of the depth of interface 15 along sections S1 (blue), S2 (red) and S3 (black). Dashed lines indicate time-averaged depth of interface 15 at each section. Horizontal and vertical axes indicate the date through model year 14 and the depth in meters, respectively.

Time series of the interfaces' depth show that higher frequency variability is superimposed on a lower-frequency signal (Fig. 5-5). At various times, the lower-frequency signal is coherent at

different locations in the DeSoto Canyon region which cannot be explained by mesoscale eddies in the area. For this reason, this part of the section focuses on large-scale upwelling and downwelling events, which occur on a spatial scale of 300–600 km and a time scale of days to weeks.

5.2.1 Cross-slope Flow Induced by Mesoscale Oceanic Eddies

This section describes the impact of oceanic eddies on upward/downward movement of water. Oceanic eddies commonly do not migrate onto the shelf because of their deep vertical structure. Eddies have a varying range of lifetimes and sizes and actively move and change their shape over the time. Demeaned SSH fields from HYCOM simulation year 14 (or 2005 in cycle 1) show that the Loop Current penetrates far north into the study domain at this time (Fig. 5-6). During January of year 14, when the position of the Loop Current front is close to 27 °N, a frontal cyclonic eddy tends to influence the deep waters off the Mississippi delta. The cyclone stays at 27.5 to 28 °N along 88.5 °W with a diameter of approximately 100 km (Fig. 5-6) and moves around the western part of the domain from January through February (Appendix A). The isopycnals underneath shoal in the cyclone's center, whereas they are depressed at its edges. A cold temperature anomaly is seen in the deeper layers (>1.5 °C), up to 1000–1200 m. One can infer that the cyclonic eddy generates uplift of the isopycnals underneath it but sinking of the isopycnals at 200 to 1200 m depths inshore and on the continental slope off the Mississippi delta.

From March through May when the cyclonic eddy merges with another frontal cyclone to the east and moves southeastward, the Loop Current starts swinging to the west and penetrating along the 88.5 °W cross-section (Fig. 5-7 and Appendix A). Strong positive SSH associated with the Loop Current spreads over the southern segment of the 88.5 °W cross-section and reaches 28 °N latitude. The isopycnals between 27 and 28 °N move downward and warm temperature anomalies are evident from the surface to 1000 m depth. On the contrary, the isopycnals on the upper slope are inclined to heave up, which is in agreement with dynamic uplift of an anticyclonic eddy described in Tomczak (1996). A cold anomaly is observed at depths of 200 to 600 m. This result is in accordance with Weisberg and He (2003) where the isopycnals move upslope as the cross-flow is directed onshore and bring the cold and rich nutrient water from the deeper layers to the slope. Once upwelling-favorable winds blow, an extensive upwelling can take place with a colder temperature anomaly of waters on a large scale over the shelf.

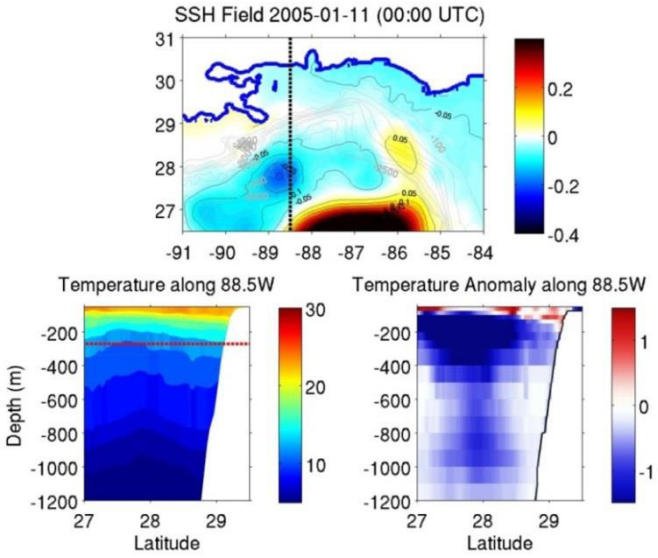

Figure 5-6: Upper figure is a snapshot of demeaned SSH on 11 January (2005 or simulation year 14) (00:00 UTC). The dashed line indicates a meridional cross section at 88.5 °W; hot color and solid contours represent positive SSH anomalies; cold color and dashed contours are negative SSH anomalies. Lower figures show temperature (°C) (left) and temperature anomaly (°C) (right) along the cross-section. The red dotted line in the lower left is a reference level for visualizing the vertical movement of isopycnals.

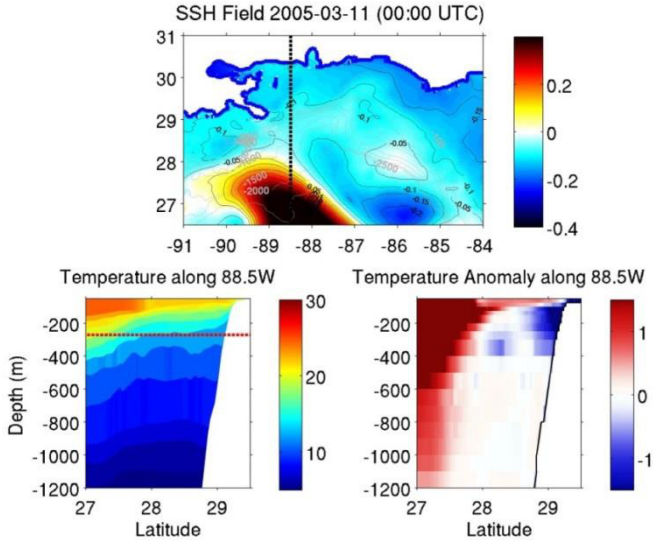

Figure 5-7: Upper figure is a snapshot of demeaned SSH on 11 March (2005 or simulation year 14) (00:00 UTC). The dashed line indicates a meridional cross section at 88.5 °W; hot color and solid contours represent positive SSH anomalies; cold color and dashed contours are negative SSH anomalies. Lower figures show temperature (°C) (left) and temperature anomaly (°C) (right) along the cross-section. The red dotted line in the lower left is a reference level for visualizing the vertical movement of isopycnals.

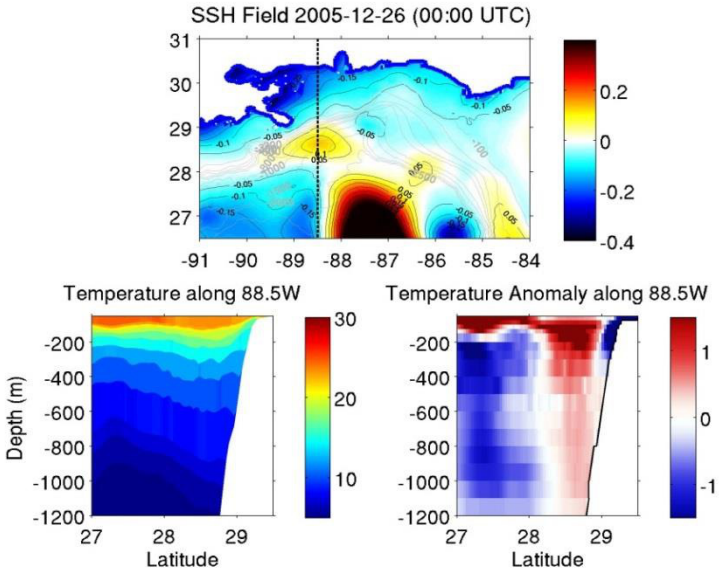

Figure 5-8: Upper figure is a snapshot of demeaned SSH on 26 December (2005 or simulation year 14) (00:00 UTC). The dashed line indicates a meridional cross section at 88.5 °W; hot color and solid contours represent positive SSH anomalies; cold color and dashed contours are negative SSH anomalies. Lower figures show temperature (°C) (left) and temperature anomaly (°C) (right) along the cross-section. The red dotted line in the lower left is a reference level for visualizing the vertical movement of isopycnals.

In December, a Loop Current anticyclonic eddy moves to the outer shelf at approximately 28.5 °N latitude and 88.5 °W longitude and stays for several weeks (Fig. 5-8). This anticyclone lowers the isopycnal underneath and raises the isopycnals at depths of 200–400 m on its shoreward periphery. Again, the cold signature is more squeezed on the upper slope, seen up to 300 m depth.

5.2.2 Cross-slope Flow Induced by the Loop Current

To identify the dominant frequencies, a spectral analysis is carried out for five selected interfaces. The results are similar between the interfaces so only analysis for interface 14 along section S1 is presented in Fig. 5-9. Two dominant low frequencies are found, equivalent to periods of 4–6 and 12 months. The first dominant period is close to the mode of the Loop Current eddy separation (Dukhovskoy et al., 2014), (Fig. 5-10). The second period is associated with the annual cycle. Movement of layer interfaces (or isopycnals) is inferred from the time-integrated vertical velocity and, low-frequency variability of layer interfaces' depth is readily obtained by filtering out high-frequency signals. The interfaces' depth is band-pass filtered with

cut-off periods of 20 and 180 days to isolate mesoscale variability possibly modulated by the Loop Current activity. The time-filtered depths are then subtracted from their mean depth to obtain a time series of depth anomaly.

Low-frequency, large-scale upwelling and downwelling events are identified by the 75th and 25th percentiles of band-pass filtered time series of depth anomaly, respectively. These events frequently occur at all three sections at the same time. To illustrate the response of the interfaces in the DeSoto Canyon region to different Loop Current regimes, two particular model years selected for analysis. These are year 14 when the Loop Current extends northward into the Gulf of Mexico and year 32 when it retracts southward. Interestingly, both model years correspond to year 2005 of atmospheric forcing but in different 18-year cycles, providing further evidence that local wind forcing is not a large contributing factor to the Loop Current extension and eddy separation. Time series of interface 15 with mean depth of 374.4 m at S1, 422.3 m at S2 and 460.3 m at S3 in these years are examined (Figs. 5-11 and 5-12) in conjunction with other model variables in order to investigate direct and remote impacts of the Loop Current on the DeSoto Canyon cross-slope flow. Large-scale upwelling/downwelling for this interface is determined and displayed as green/orange markers and their time periods are objectively detected.

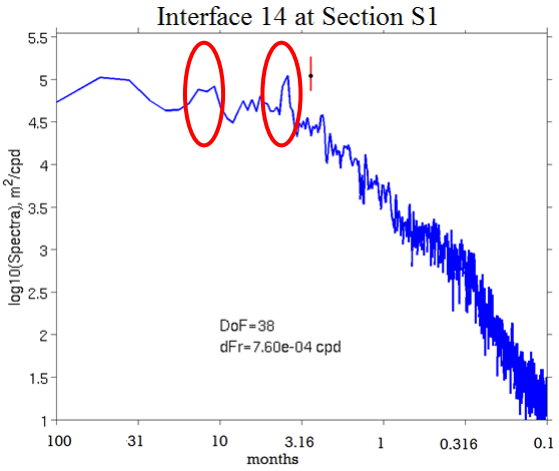

Figure 5-9: Spectral analysis of the depth of interface 14 at section S1. There are DOF = 38 and frequency resolution dFr = 7.6e-04 cpd. Vertical and horizontal axes represent log base 10 of spectra and time periods in months, respectively. Red ovals indicate peaks of spectra.

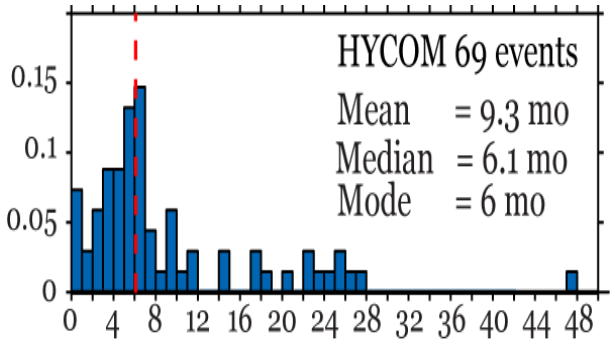

Figure 5-10: Histogram of the Loop Current eddy separation period from the multi-decadal HYCOM simulation. (Dukhovskoy et al., 2014).

In simulation year 14, there exist five to eight upwelling or downwelling events (blue markers) (Fig. 5-11), only three to five of which are large-scale. Large-scale downwelling (orange) occurs in the periods 10 March–2 April (D1), 11–15 August (D2) and 10–25 September (D3) and large-scale upwelling takes place during 21 January, 12–21 February, 11–29 July, 20–25 October and 16–25 November. In simulation year 32, there are three large-scale downwelling events during 21 April–29 May (D1), 31 July–14 August (D2) and 27 September–13 October (D3) (Fig. 5-12) and four large-scale upwelling events during 2–6 February, 21 February–5 March, 28–29 March, and 7 June–25 July. Further, large-scale upwelling and downwelling ranges from tens to over one hundred meters. The retracted Loop Current remotely drives a stronger downwelling than the extended Loop Current. For interface 15, the maximum vertical distance is about ± 100 to 120 m for year 32, e.g. the event D1 and ± 70 to 80 m for year 14 (Figs. 5-11 and 5-12), e.g. the events D1 and D3.

To assess how the Loop Current activity can impact vertical circulation on the slope, the demeaned SSH field during the large-scale upwelling and downwelling periods in these years in the eastern Gulf of Mexico is examined. The Loop Current penetrates far into the Gulf of Mexico with its northern front reaching up to 27–27.5 °N and 88–89 °W in the beginning of year 14. A series of strong frontal cyclonic eddies moves in the clockwise direction and impacts the northward development of the Loop Current. The Loop Current stretches out to section S3 in the eastern part of the DeSoto Canyon domain, slightly sweeps from Tampa Bay to Naples and drifts more westward. It starts to change orientation to southeast-northwest in the beginning of March (Fig. 5-13a); on March 10th its northern edge is located at 27.8 °N and 90 °W, off the Mississippi delta while the eastern edge impinges upon the continental slope offshore of Naples. At this time, a strong cyclonic eddy occurs at 26.5 °N and 86 °W and has a tendency to head south-southwestward. The cyclone causes the Loop Current to spread further eastward and strongly hit the west Florida shelf during middle March through early April (Figs. 5-13b and c). A band of strong positive SSH anomaly extends northward from the Loop Current near the impingement point. In the meantime, the Loop Current continues developing northward, so its northern edge intrudes into the study domain from the southwest. A combination of these two effects seemingly results in the first large-scale downwelling period D1 (Fig. 5-11). After shedding a large anticyclonic eddy on April 14th, the Loop Current's northern front stays at approximately 26 °N and 87.5 °W and keeps extending toward the study domain. In July, the Loop Current and its

frontal cyclonic eddies spread in the deeper portion. An incomplete detachment occurs when a strong peripheral cyclone moving clockwise toward Naples cleaves the Loop Current. Another energetic cyclone located at 28 °N in the middle of the deep water region also distorts the Loop Current from the north. Consequently, in August the Loop Current spreads out in the east-west direction so that its western edge reaches 90 °W while its eastern edge impinges upon the continental shelf of the Tampa Bay (Fig. 5-13d). In the middle of August, propagation of a small portion of the Loop Current from the contact point on the west Florida shelf and direct intrusion of the Loop Current northern edge again (Figs. 5-13e and f) occur and work together to cause the second large-scale downwelling D2 over the slope (Fig. 5-11). On August 19th, an anticyclonic eddy is separated from the Loop Current by necking down of two peripheral cyclones. Later these cyclones are merged into a bigger cyclone, expanding in the middle of the eastern Gulf of Mexico at latitudes of 25–27.5 °N and longitudes of 86–89 °W and pushing the Loop Current to the east. Accordingly, the third impingement of the Loop Current takes place and results in a break off of a small anticyclone in early September. High pressure extending over the region from the remote influence of the Loop Current impingement on the west Florida shelf, as well as a persistent anticyclone in the region, lead to event D3.

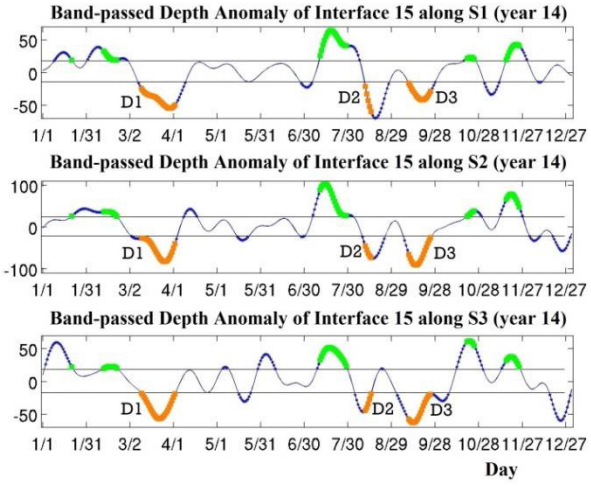

Figure 5-11: Band-pass filtered depth anomaly of interface 15 along three sections S1, S2 and S3 in simulation year 14. Green markers indicate large-scale upwelling periods; orange markers show large-scale downwelling periods (D1, D2 and D3). Two solid black lines are the 25th and 75th percentiles.

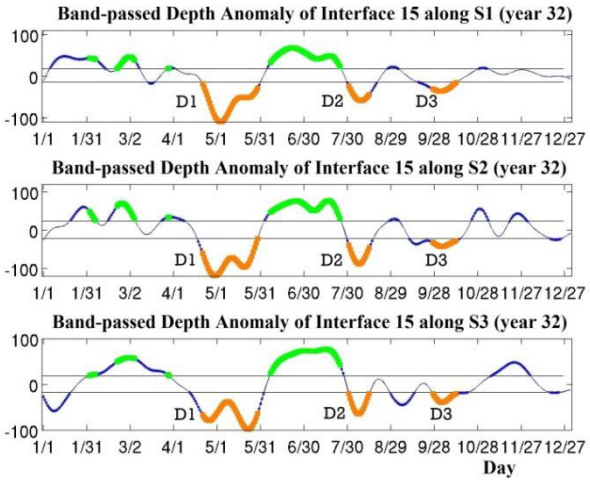

Figure 5-12: Band-pass filtered depth anomaly of interface 15 along three sections S1, S2 and S3 in simulation year 32. Green markers indicate large-scale upwelling period; orange markers show large-scale downwelling periods (D1, D2 and D3). Two solid black lines are the 25th and 75th percentiles.

In simulation year 32, the Loop Current only slightly penetrates in the eastern Gulf of Mexico. Its northern front mostly stays south of 26 °N latitude, close to south of the west Florida shelf; a large frontal cyclonic eddy hinders northward development of the Loop Current. In the period of late March–early April, the Loop Current protracts further northward, up to 25.5–26 °N and a cyclonic eddy in front of the Loop Current's western boundary grows stronger and squeezes the Loop Current to the east, leading to the first hit on the slope of Fort Myers on April 18th (Fig. 5-14a). Following this, the Loop Current has a tendency to stretch to the north and even sheds small anticyclonic eddies along the west Florida slope and shelf and, for over a month, into the DeSoto Canyon region (Figs. 5-14b and c). The remote high pressure of the Loop Current appears to govern the continental slope circulation and produces a persistent and strong downwelling event D1 during April through May of year 32 (Fig. 5-12). Similarly, the Loop Current impinges upon the west Florida slope in July–August and in September–October, and is responsible for other large-scale downwelling events in the corresponding periods. In particular, in both cases, there is a Loop Current related anticyclonic eddy (with a diameter of about 100 to 200 km) offshore of Naples which drifts along the west Florida slope into the DeSoto Canyon region. These eddies can survive for several months and contribute to generation of the large-scale downwelling events on the continental slope.

To assess how the Loop Current remotely induced high pressure propagates into the domain, Hovmöller diagrams are constructed for SSH anomaly along seven isobaths of 100, 200, 300, 500, 700, 1000 and 1500 m from the Florida Straits to the Mississippi delta in two model years, 14 and 32 (Fig. 5-15 and Appendix B). The large-scale upwelling and downwelling periods are shown with the pink and blue boxes, respectively. In model year 14, the extended Loop Current contacts the west Florida shelf further north more frequently, although only some contacts generate a high pressure band extending toward the domain. Strong positive SSH anomalies (>0.16–0.17 m) are clearly seen at irregular intervals over the deep isobaths of 1000 and 1500 m (Fig. 5-15a); sometimes the contact can endure for weeks to months. A band of strong positive SSH anomaly is directed southwest-northeast from 800–900 km to 400 km along the 1000 m isobath during February–April and July–October. This is related to north-to-south sweeping of the Loop Current along the west Florida shelf. Three large-scale downwelling periods (blue boxes) are shown to have a high positive SSH band at distances between 400 and 600 km (from Key West to north of Fort Myers) and at distances 1300–1400 km (southwest of the Mississippi

River mouth) along all isobaths from 300 to 1500 m. This supports the idea that the large-scale downwelling is generated by double impingements of the Loop Current or the combined remote and direct influences of the Loop Current in year 14. Nonetheless, the shallower isobaths indicate a seemingly continuous positive SSH at distances from 400 to 1400 km (from Key West to the Mississippi delta) during these downwelling periods (Figs. 5-15b and c), especially along the 300 m isobaths although the magnitude of SSH anomaly can be smaller along this isobaths. This implies that the Loop Current remotely induced high pressure tends to propagate along the outer shelf isobaths.

The remote influence of the Loop Current is more evident in Hovmöller diagrams of SSH anomaly for model year 32 (Figs. 5-15d, e and f). The SSH anomaly field is higher (more positive) compared to year 14. For most of the year, the Loop Current interacts with the southern west Florida shelf shown by a very strong SSH anomaly band (0.12–0.2 m) at distances from 300 to 450 km. This band is not uniform for the deep isobaths of 1000 to 1500 m for the downwelling periods. However, there is a distinct SSH band at distances from 300 to 1400 km or over the entire west Florida shelf through to the Mississippi delta along the 100 to 500 m isobaths for all large-scale downwelling periods of model year 32 (Figs. 5-15e and f).

To obtain statistical results of the large-scale, low-frequency events, time- and space-averaged SSH for the upwelling and downwelling is estimated over the 36 year simulation period. 146 large-scale downwelling events and 137 large-scale upwelling events are detected for interface 15. The isobaths of 100 to 1500 m from the Florida Straits to the Mississippi delta are divided into two segments which are located inside (black) and outside (green) the DeSoto Canyon domain (Fig. 5-16). Mean SSH anomaly is calculated for these isobaths and displayed in Fig. 5-17. In general, the downwelling is associated with positive SSH anomaly and the upwelling corresponds with negative SSH anomaly. It reflects well the high and low pressures causing vertical circulation on the continental slopes. Mean SSH changes between segments inside and outside the domain as well as between the isobaths. Its magnitude along the segments inside the domain is smaller than that along the segments outside. It is reasonable, since the low-frequency high pressure can be weakened or dissipate on its pathway and also there is a higher chance of the Loop Current interaction with the southern portion of the west Florida shelf.

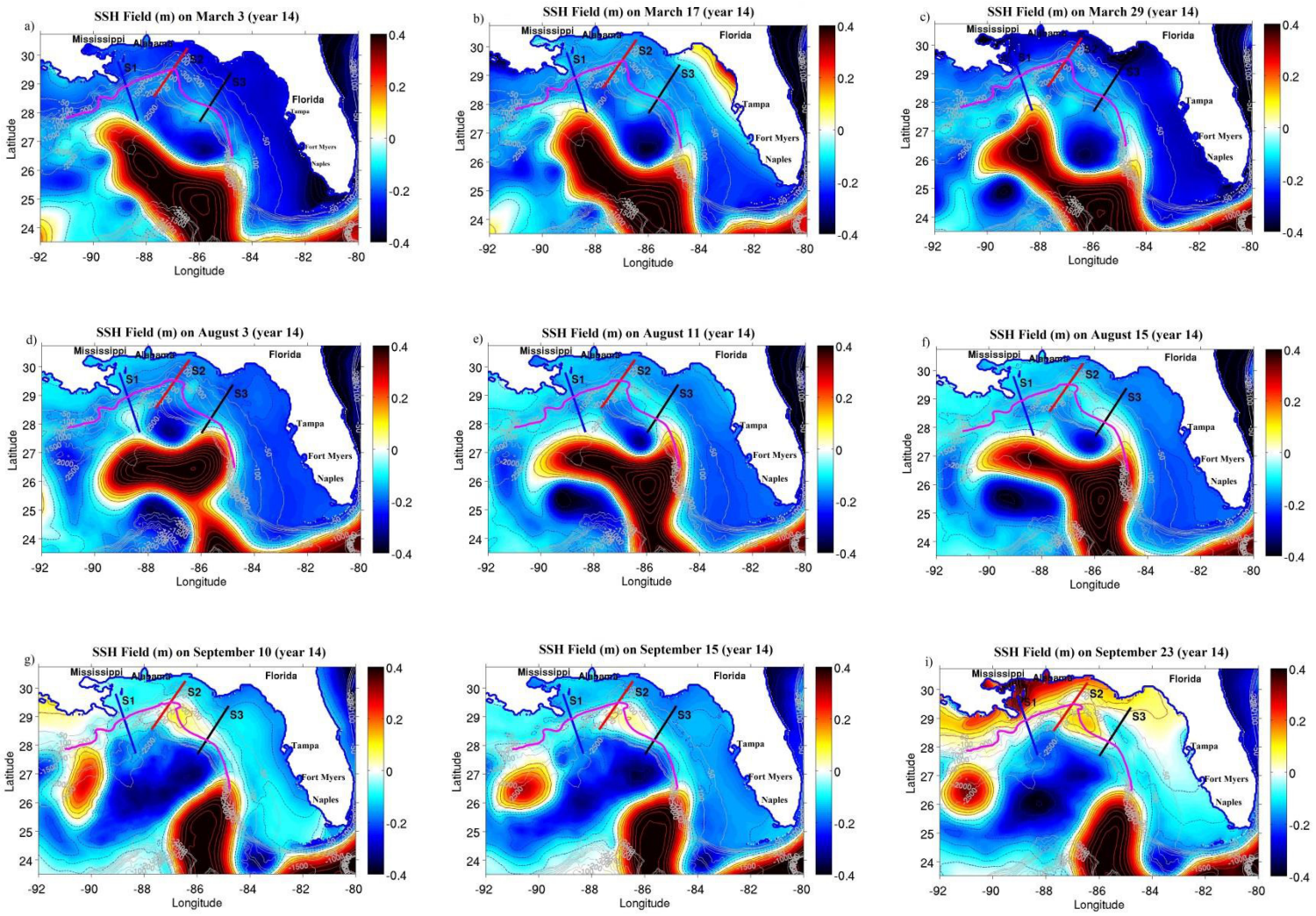

Figure 5-13: Snapshots of demeaned SSH in large-scale downwelling events in simulation year 14 in the eastern Gulf of Mexico. Blue, red and black lines across the continental slope denote sections S1, S2 and S3, respectively. The magenta contour is interface 15. Gray contours are depth contours. Dashed blue and solid red contours show negative and positive SSH, respectively.

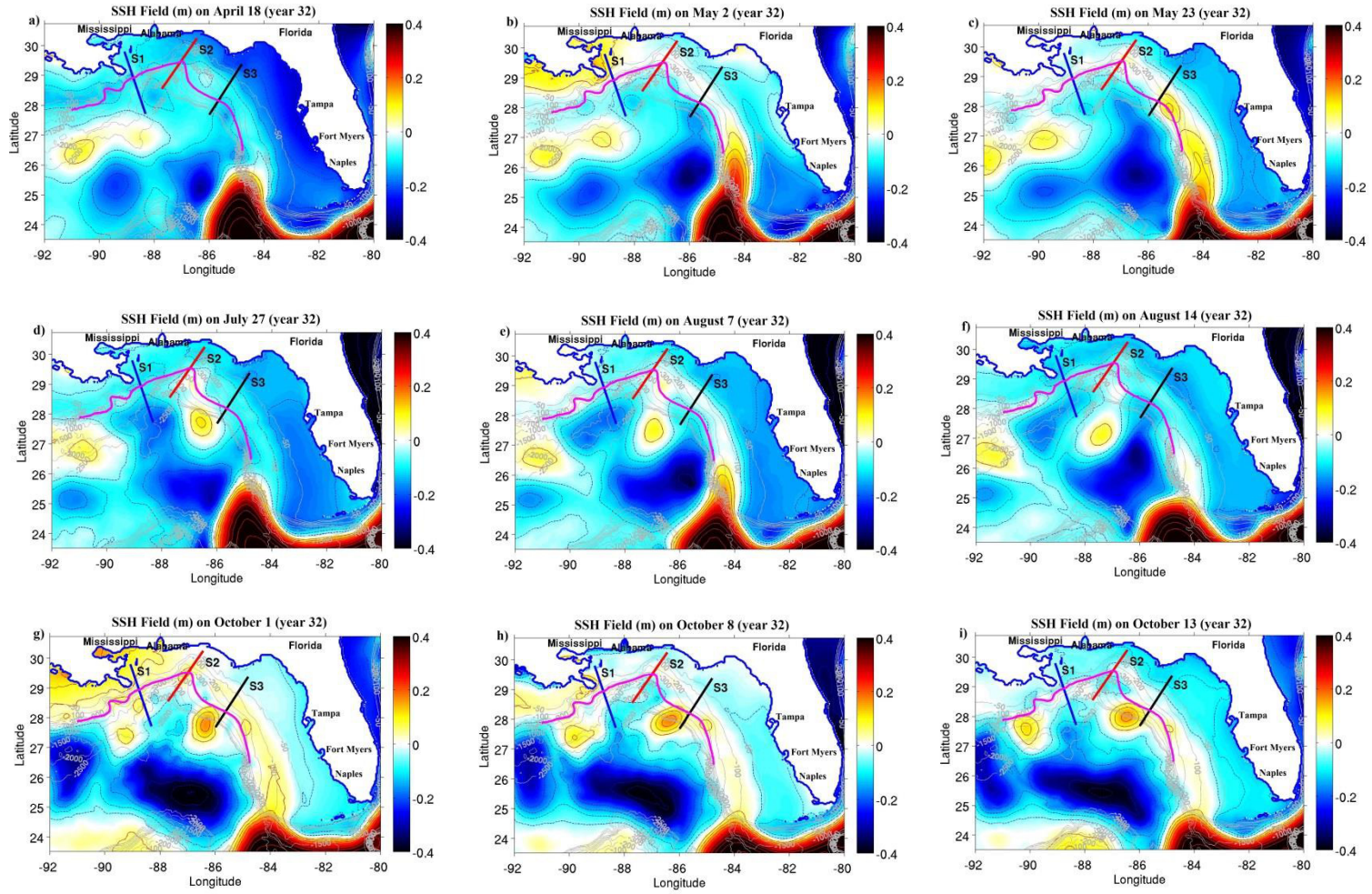

Figure 5-14: Snapshots of demeaned SSH in large-scale downwelling events in simulation year 32 in the eastern Gulf of Mexico. Blue, red and black lines across the continental slope denote sections S1, S2 and S3, respectively. The magenta contour is interface 15. Gray contours indicate depth contours. Dashed blue and solid red contours show negative and positive SSH, respectively.

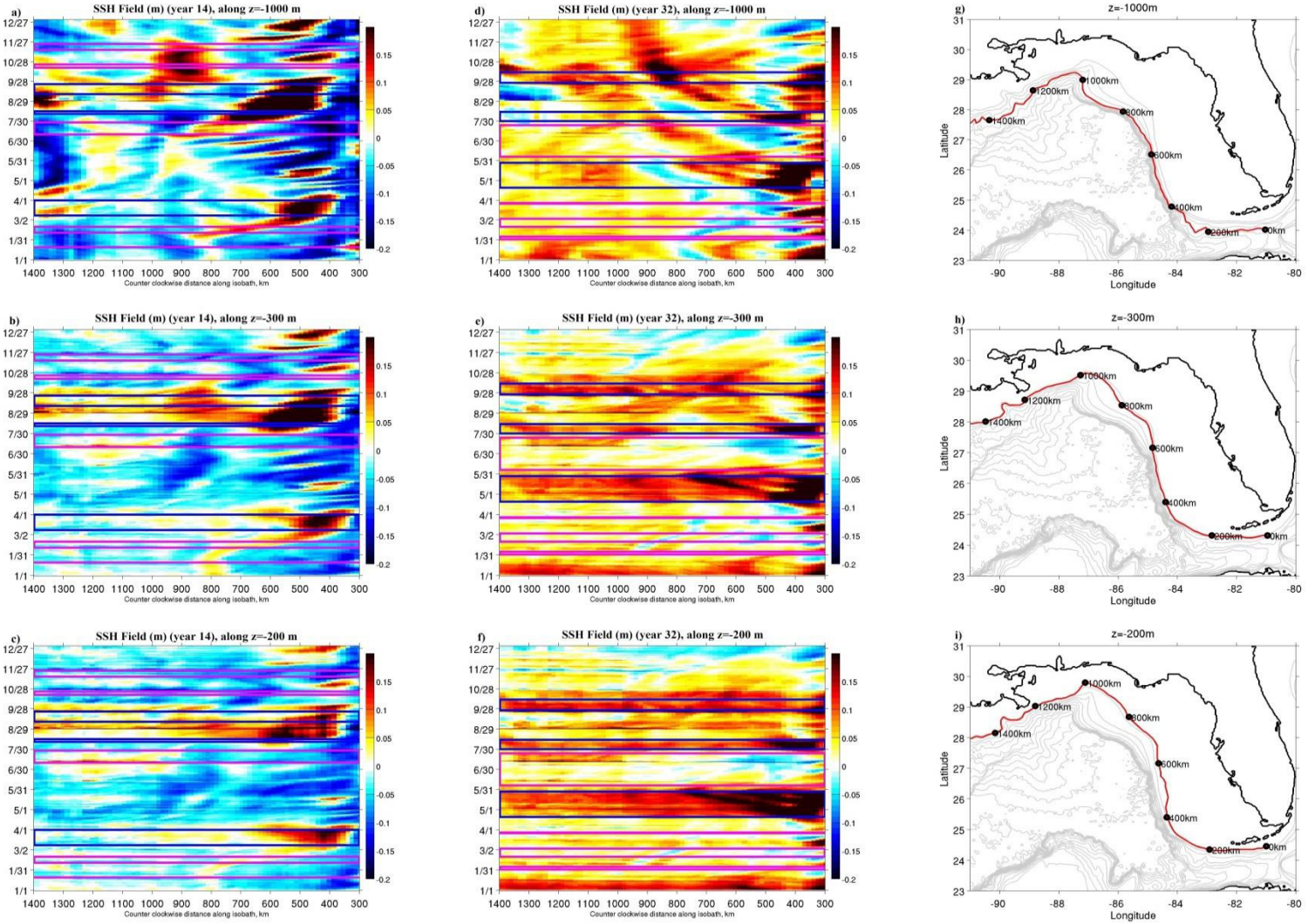

Figure 5-15: Hovmöller diagrams of SSH anomaly along the 200, 300 and 1000 m isobaths in simulation year 14 (a, b, c) and year 32 (d, e, f). Color indicates SSH value. The horizontal axis is the distance along the isobaths and the vertical axis is the date ranging from 1 January to 31 December. Maps of distance along the isobaths (g, h, i). The pink/blue boxes indicate upwelling/downwelling periods.

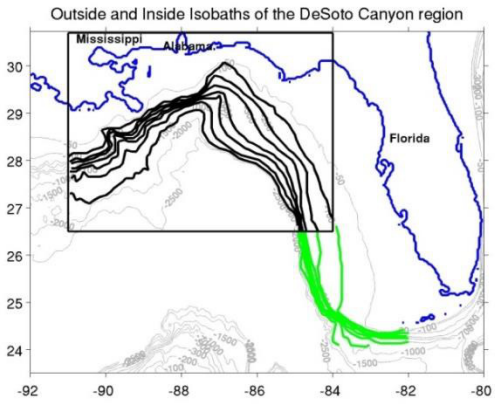

Figure 5-16: Isobath segments inside (black) and outside (green) of the DeSoto Canyon domain.

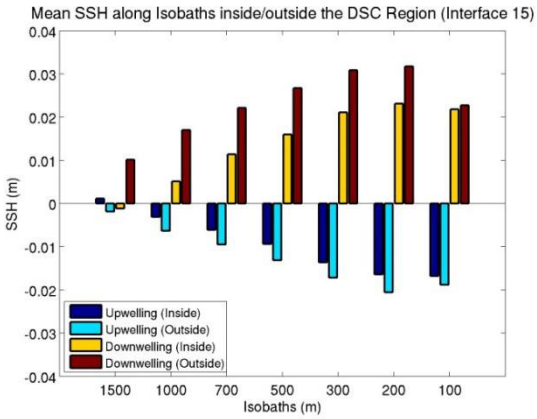

Figure 5-17: Time-averaged SSH anomalies during large-scale upwelling (dark and light blue) and downwelling (yellow and brown) events along the isobaths inside and outside the DeSoto Canyon domain over 36 years of the HYCOM simulation.

The difference between the inside and outside SSH anomalies reduces as the isobaths become shallower for both upwelling and downwelling cases. This is due to a higher chance of oceanic eddies disturbing the deeper isobaths. The mean inside SSH has a maximum value of about 0.02 on the 200 m isobath and a minimum value of about -0.001 m on the 1500 m isobath. The outside SSH magnitude can double the inside SSH, e.g. for the 500 to 1500 m. In addition, the mean SSH magnitude is smaller (-0.02) for the upwelling than for the downwelling (>0.03).

5.3 Characteristics of Upwelling and Downwelling

Unfiltered daily time series of intersection of model layer interfaces with the bottom slope across sections S1, S2 and S3 used in Section 5.2 are analyzed in this section to provide statistical descriptions of the upwelling and downwelling across the continental slope of the DeSoto Canyon region. This section describes the distribution of several parameters of the upwelling and downwelling including vertical and horizontal displacements and event durations, which are of significant concern for marine species and water quality.

5.3.1 Vertical Excursion

The time series of daily depth anomaly of intersection between the model interfaces and the sea floor across the three sections are estimated by subtracting time-averaged depth of the interfaces from daily time series of depth. Positive and negative anomalies indicate the upwelling

and downwelling of the interfaces, respectively. Normalized histograms of the depth anomalies are derived for interfaces 14 and 16 for the period of 36 years and shown in Fig. 5-18 to reveal variability of vertical excursions at three different locations. Other histograms for interfaces 15 and 18 can be found in Appendix C.

Distributions of vertical excursion substantially change among sections, primarily depending on local characteristics such as local topographic slopes and governing ocean dynamics. According to Hsu (1999), winter cylogenesis and frontal overturning can generate a vertical rate of 1.8 m per day, therefore events with a vertical distance of over 30 m are considered strong events. For interface 14, the distribution looks bimodal at all sections S1, S2 and S3, although two peaks are more prominent along S2. (Figs. 5-18a to c). The distribution becomes broader from S1 to S3 (west to east) with the standard deviation varying from +30.8 m at S1 to +38.6 m at S3. The median value is small, -2.5 m at S1 and -1.3 m at S3, indicating that the downwelling has a little slightly higher chance of occurrence than the upwelling (0.53 to 0.56). The distribution is positively skewed at section S2; upwelling events have a probability of 0.57 and there are two prominent modes in the intervals [+5 +10] m and [-35 -30] m. Vertical distance range (the 10^{th} and 90^{th} percentiles) falls into the interval of -49 to +51 m at S1, -38 to +34 m at S2 and -39 to +40 m at S3 and can be as high as ± 100 m. Upwelling distances of 0 to 30 m occur about 45 % of the time at S2, 29 % at S1 and 26 % at S3 and downwelling distances of 0 to 30 m occur 39 % of the time at S1, 29 % at S3 and 18 % at S2. This result shows that upwelling for interface 14 is more likely to take place over the canyon and the downwelling is prone to occur at S1. There is a 21 % chance of strong upwelling events with vertical distance being greater than 30 m occurring at section S3, and about 12 to 15 % chance at sections S1 and S2. Otherwise, the chance of occurrence for strong downwelling events appears higher, about 24 % at S3, 25 % at S2 and 17 % at S1. Despite a small chance, stronger downwelling events with vertical distance being greater than 50 m are more likely to take place at S3 than at S1 and S2, for example 11.3 % at S3 but 5 to 6 % at S1 and S2 for downwelling events. Yet stronger upwelling events are less likely to occur with chance of occurrence less than 10 % at all sections.

Going deeper, vertical excursions of interface 16 exhibit a multi-modal distribution at all sections (Figs. 5-18d to f), with distributions tending to be broader at S1 and S2 and narrower at S3 compared to that of interface 14. Vertical distance ranges from -53 (the 10^{th} percentile) to +56 m (the 90^{th} percentile) and may reach up to ± 80 to ± 100 m. The distribution looks bimodal and

symmetric with two distinct modes in the absolute interval [45 50] m at S1, and somewhat positively skewed at other sections.

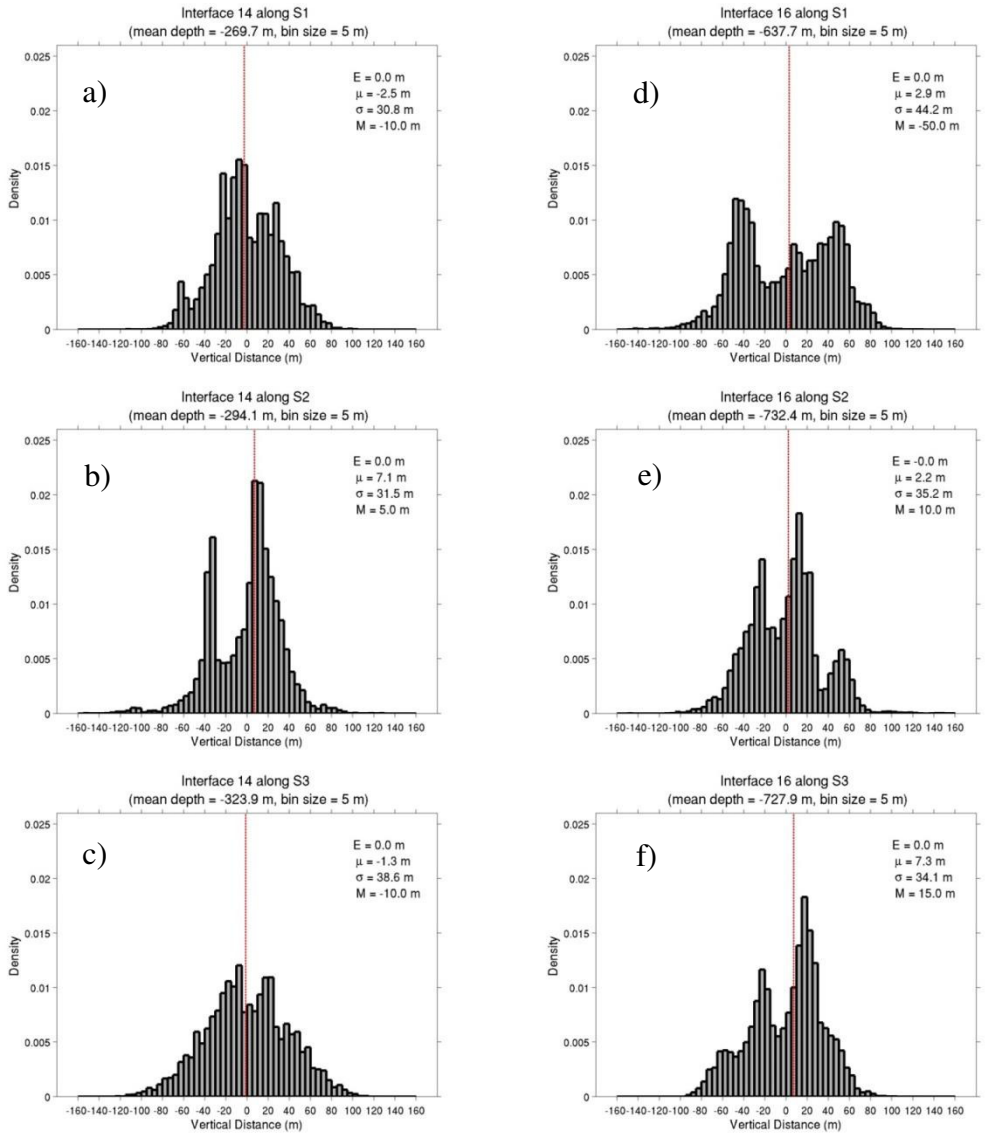

Figure 5-18: Normalized histograms of vertical excursion of interfaces 14 (a, b, c) and 16 (d, e, f) at sections S1, S2 and S3 with a bin size of 5 m. The dashed red line indicates the median; E is mean value, μ is the median, σ is standard deviation and M is the mode. Horizontal and vertical axes are vertical distance in meters and probability density, respectively.

The positive mode has higher probability density in [+10 +15] m at S2 and [+15 +20] m at S3 than the negative mode in [-25 -20] m. Upward distance of between 0 and 30 m has a chance of about 39 % at S3, 35 % at S2 and 20 % at S1, whereas the same downward distance has a smaller chance of about 24 % at S3, 28 % at S2 and 13 % at S1. In particular, there is a significant chance for stronger upwelling and downwelling with vertical distance greater than 30 m at all sections, such as 22 % at S3 and S2 and 37 % at S1 for downwelling and 14 to 16 % at S3 and S2 and 30 % at S1 for upwelling. Vertical distances of greater than 50 m have a chance of occurrence of 15 % at S1 for downwelling and 14 % at S2 for upwelling.

In general, the distribution for interface 14 may result from wave-like motions such as internal topographic waves. Bimodal and multi-modal distributions for the deeper interfaces possibly present individual up and downwellings. The greater mode would be related to an enhanced effect of the persistent wind and the oceanic eddy or a wide range of oceanic eddy configurations that may favor either upwelling or downwelling conditions. Interface 14 moves over a maximum distance of approximately 80 to 120 m at the sections, comparable with the isopycnal displacement associated with the Loop Current, as discussed in Section 5.2.

In addition, oceanic eddies have a vertical extension of several hundreds to a thousand meters, likely influencing interfaces 14 and 16. Coria-Monter et al. (2014) and Vaillancourt et al. (2003) found that isopycnal surfaces can obtain an uplift of about 30–60 m at depths of 100 to 120 m due to a cyclonic eddy. Wind-driven upwelling can extend further offshore to depths of 200 to 300 m at the canyon's head and on the eastern shelf of the DeSoto Canyon region, and thus the wind may account for the weaker but more frequent upwelling being smaller than 15 m along sections S2 and S3 (Figs. 5-18b, e and f).

5.3.2 Horizontal Excursion

Horizontal excursion is of critical importance for fishermen and ecologists, because this parameter can represent how far larvae and juveniles of marine organisms as well as polluted material can disperse offshore and onshore and, therefore, how the upwelling-associated high productivity area spreads over the continental slope. The horizontal distance of the layer interface intersection with the slope is computed with respect to the offshore endpoints of sections and the time series of the excursion anomalies are constructed and analyzed for the three sections. Positive/negative value indicates shoreward/seaward movement. Normalized

histograms of the horizontal distance in kilometers for interfaces 14 and 16 are depicted in Fig. 5-19.

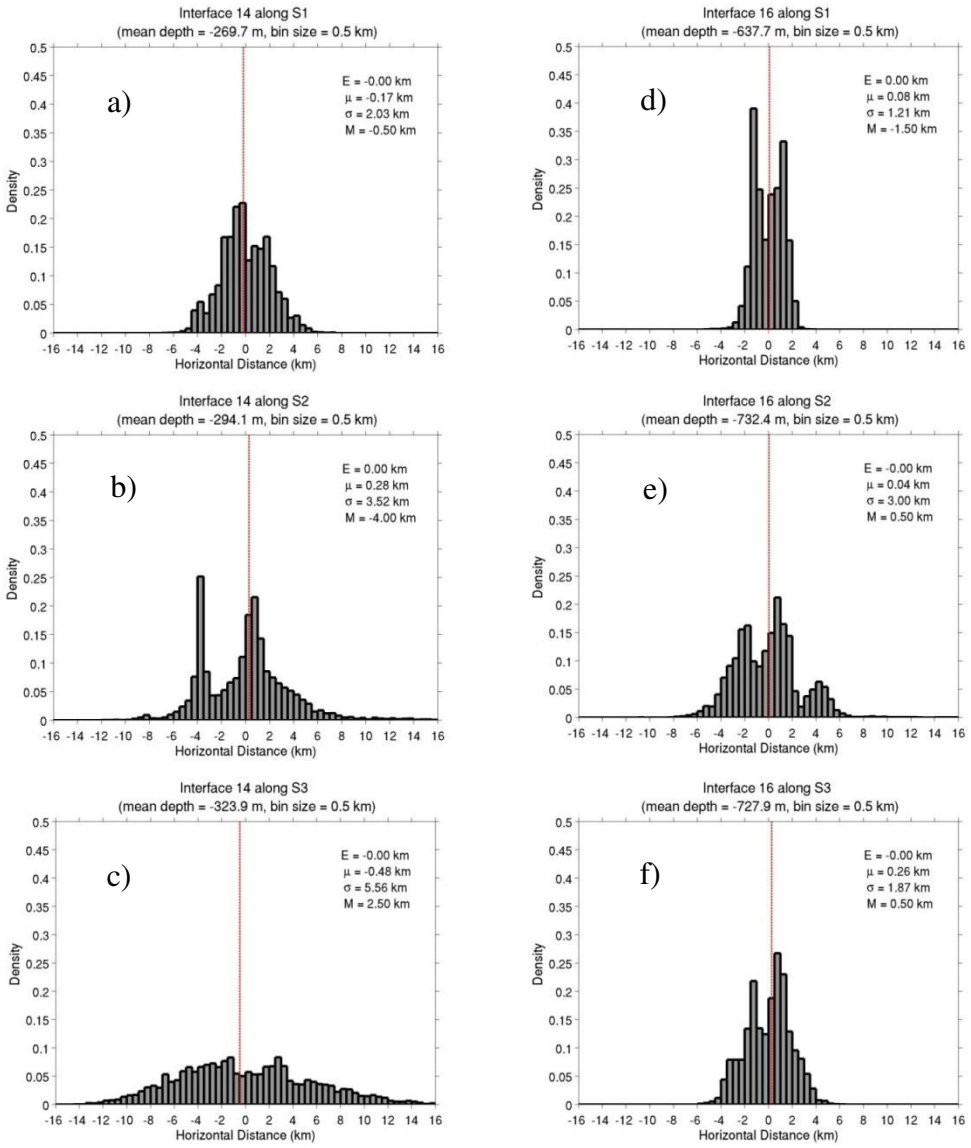

Figure 5-19: Normalized histograms of horizontal excursion of interfaces 14 (a, b, c) and 16 (d, e, f) at sections S1, S2 and S3 with a bin size of 0.5 km. The dashed red line is the median. E is mean value, μ is the median, σ is standard deviation and M is the mode. Horizontal and vertical axes are horizontal distance in kilometers and probability density, respectively.

In general, these histograms of horizontal excursion are relatively similar to the vertical excursion, e.g. bimodal at all sections for interface 14. The width of the distribution is much

different among sections, substantially depending on the topography gradient. A fairly broad distribution of the depth of the intersection of interface 14 with the slope occurs at S3 with a standard deviation of 5.56 km. Here the topographic slope is gentler than along S1 and S2 (Figs. 5-19a to c) and the distance ranges from approximately -6.91 (the 10^{th} percentile) to +7.6 km (the 90^{th} percentile). The range of the distance is noticeably reduced, from -2.54 to +2.6 km at S1 and from -3.96 to +4.13 km at S2, corresponding with the 10^{th} and 90^{th} percentiles. Thus, the chance for an excursion of less than 4 km is about 52 % at S1, 35 % at S2 and 27 % at S3 in the seaward direction, but approximately 41 % at S1 and S2 and 24 % at S3 in the shoreward direction. Otherwise, the chance for the excursions exceeding 6 km is about 14 to 15 % along S3, but negligible along other sections. The modes for section S2 are pronounced in the intervals [-4 -3.5] and [+0.5 +1] km.

Interface 16 has a multi-modal and narrow distribution with a standard deviation of 1 to 3.5 km and a smaller range for all sections (Figs. 5-19d to f). The excursion is highest at S2 with 7.5 to 8 km, but about 3 km at S1 and 5 km at S3 (between the 10th and 90th percentiles). The chance for the seaward and shoreward distance of 3 km to occur is about 54 % at S1, 37 % at S2 and 40 % at S3, and about 46 % at S1, 34 % at S2 and 47 % at S3, respectively. There is a chance of 12 to 15 % for the distance exceeding 3 km at S2.

5.3.3 Upwelling and Downwelling Duration

All upwelling and downwelling events which persist longer than a day are taken into consideration. Event duration (in days) is estimated from time series of the depth anomaly using the criteria that the anomalies lie outside the 75^{th} and 25^{th} percentiles. Normalized histograms of the event duration for interfaces 14 and 16 are illustrated in Fig. 5-20, those for other interfaces are in Appendix D. These distributions have the mode of 1 to 2 days and mostly range from 1 to 29 days for interface 14 and from 1 to 18 days for interface 16. One- to six-day events have the chance of occurrence of 45 to 57 % for interface 14 and more than 60 % for interface 16. The long tail of these distributions indicates the possibility of long-period events and the probability events exceed a two-week duration is approximately 20 to 30 % for interface 14 and 10 to 13 % for interface 16.

To examine duration of the long-period events, normalized histograms of the duration for the large-scale events which are defined as in Section 5.2.2 are shown in Fig. 5-21. The histograms

look different from the general events. Their distributions greatly shift to the longer period and become broad for all interfaces. The mode is located in the interval of 6 to 14 days and the event duration varies from 3 to 30 days for interface 14 and from 4 to 27 days for interface 16 (the 10th and 90th percentiles). A chance of the events with duration exceeding 14 days is about 40 % for interface 14 and 30 % for interface 16. More persistent upwelling events for over 21 days have a chance of occurrence of 22 to 24 % for interface 14 and a smaller chance for interface 16.

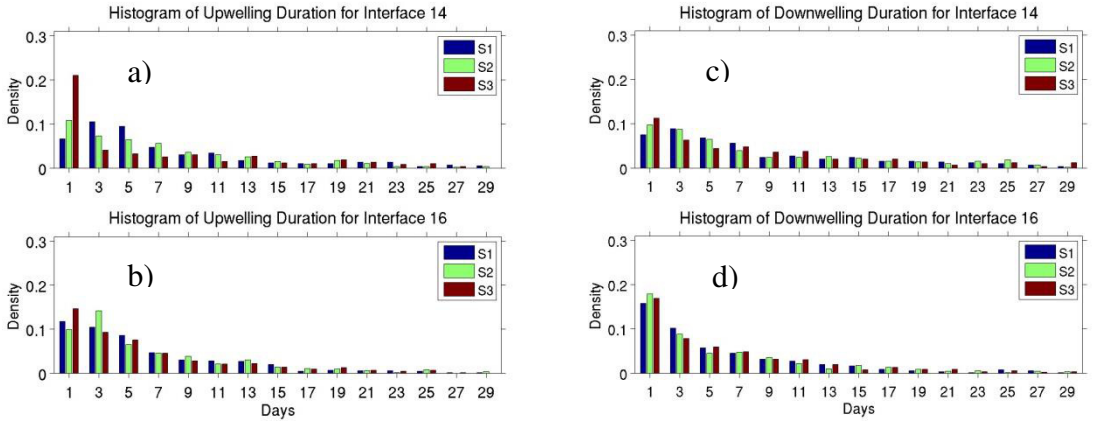

Figure 5-20: Normalized histograms of upwelling (a, b) and downwelling (c, d) duration for interfaces 14 and 16. Horizontal and vertical axes indicate duration in days and probability density, respectively.

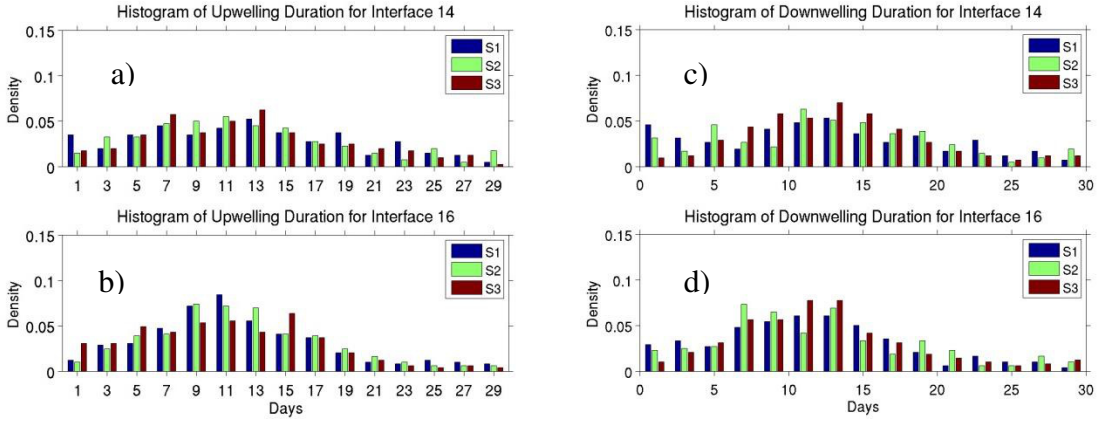

Figure 5-21: Normalized histograms of duration of the large-scale upwelling (a, b) and downwelling (c, d) induced by mesoscale circulation for interfaces 14 and 16. Horizontal and vertical axes are duration in days and probability density, respectively.

CHAPTER 6

CONCLUSION AND DISCUSSION

This study investigates the upwelling and downwelling associated with the cross-slope flow in the DeSoto Canyon region using multi-decadal GoM-HYCOM model outputs. Instantaneous vertical velocity and vertical movement of the isopycnals are estimated and examined considering local winds and the oceanic eddy field. The estimated correlation between vertical velocity and along-isobath wind component is not high; poor correlation is present close to curvatures of the isobaths such as along the western rim of the canyon, off the Mississippi delta and Apalachicola Bay. This suggests that curved coastlines complicate wind-driven upwelling and downwelling processes. When the wind field is assumed to be approximately uniform over the DeSoto Canyon region and the west Florida shelf over time scale comparable to the setup of the upwelling and downwelling, an analysis may be carried out for the time series of vertical velocity and the wind to find the most effective wind direction in the domain. It is found that the most effective winds causing upwelling are northwesterly for the continental shelf from Cape San Blas to the Mississippi delta. This wind direction is more or less perpendicular to the isobaths of the western shelf, which is not correct for Ekman-driven upwelling. Moreover, the DeSoto Canyon is relatively broad with the isobath's curvature greater than the internal deformation radius; the flows travel almost exactly along the isobaths and the wave-like response to the wind on the west Florida shelf undoubtedly passes through the canyon. This substantiates the claim that the upwelling west of the canyon results from the free-propagating shelf waves which are remotely generated on the west Florida shelf. Here, the upwelling-favorable wind is directed almost exactly along the isobaths on the eastern shelf. In addition, the wind-driven upwelling is primarily concentrated on the inner and middle shelf off Alabama and the Mississippi delta but expands to the outer shelf and the slope off the Florida Panhandle. The time lag between the effective wind component and the near-bottom cross-slope velocity is computed and ranges from several hours to approximately a day within the domain.

Another important finding is that mesoscale processes result in large-scale, low-frequency events on the DeSoto Canyon continental slope. Local eddies with different sizes and lifetimes have a high chance of influencing vertical movement of isopycnals when they approach the slope. Shoaling/deepening of isopycnals is found underneath a cyclonic/anticyclonic eddy, and

above all isopycnals on the eddy's periphery behave in an opposite way. The isopycnals are pressed on the shelf edge, and therefore, dynamic uplift (depression) is seen in case of an anticyclone (cyclone). This result explains the large-scale upwelling event in 1998 in the study domain and supports the study of this event in Weisberg and He (2003). In the same way, when the Loop Current reaches the slope, downwelling can take place beneath but upwelling can occur on the outer shelf. Even if the Loop Current retreats southward and impinges upon the west Florida shelf, it greatly influences the DeSoto Canyon slope through producing a high pressure gradient along the shelf. As a result, large-scale, long-period downwelling events arise over the entire slope. Analysis of Hovmöller diagrams of sea surface height indicates that the remote high pressure propagates along the shallow isobaths of 100 to 300 m toward the study domain and the pressure disturbance is higher for the impingement point located further south of the west Florida shelf. This finding is in agreement with Hetland (1999).

Characteristics of the upwelling and downwelling are obtained, analyzing the time series of the depth anomaly of the intersection of isopycnals and seafloor at three cross-sections over a simulated period of 36 years. Generally, vertical and horizontal excursions have a bimodal distribution for interface 14 at three cross-sections S1, S2 and S3. Although these excursions are substantially different among sections and interfaces, for interface 14 with mean depth of approximately from 250 to 325 m, vertical excursions mostly vary from ± 35 to ± 50 m and horizontal excursions change from ± 2.5 to ± 7.5 km, respectively. Greater excursions of ± 100 m or ± 10 to ± 14 km are more probable for interfaces 14 and 16. These may be associated with mesoscale circulation which can be modulated by the energetic Loop Current.

Duration of the upwelling and downwelling on the slope is estimated and primarily ranges from 1 to 29 days for interface 14 and from 1 to 18 days for interface 16. The most frequent duration lies between 1 and 2 days, but there is a significant chance for persistent events. The probability for events of exceeding a two-week duration is about 20 to 30 % for interface 14 and over 10 % for interface 16. Furthermore, large-scale, low-frequency events modulated by the Loop Current and its eddies most frequently have duration of 6 to 14 days. Persistent upwelling and downwelling events are of ecological importance because they can dramatically modify physical and chemical conditions of waters, which are controlling factors for recruitment and growth of marine organisms. In addition to boosting marine productivity, a persistent upwelling can cause adverse consequences, for examples hypoxia related to the upwelling event in 1998

and red tides. Moreover, persistent events can transport larvae and juveniles of fishes and invertebrates farther away from their natural habitat, reducing their survival chance.

As discussed in Section 2.3, the DeSoto Canyon is relatively broad compared with other canyons concerned in previous studies. As the radius of the isobath curvature is also greater than the internal deformation radius, the canyon can be considered an extension of the west Florida shelf and flow patterns go approximately along the isobaths. Change in relative vorticity, when flows move along the canyon's flank, may not happen frequently for the DeSoto Canyon. In addition to the wind, continental shelf dynamics within the DeSoto Canyon region are primarily controlled by river inflows. There are about 16 rivers with a large freshwater input. The Mississippi River, the world's third largest river, supplies a tremendous amount of 14000 m^3/s of freshwater and other rivers contribute about 4415 m^3/s. River discharges are usually greatest during the springtime, when snow melts on the land, e.g. 27000 m^3/s for the Mississippi River in February. Together with seasonal changes of surface heat fluxes, the freshwater inputs considerably modify water stratifications which can interfere with the wind effect in the study domain. In particular where water depths are quite small, the Ekman layer may not be fully developed. This can be an explanation for a poor coherence between the along-isobath wind component and the near-bottom vertical velocity off the Mississippi delta and around Apalachicola Bay.

Further work should focus on analyzing time scales of wind-driven upwelling and downwelling, with an emphasis on upwelling and downwelling set up and propagation time of distant free waves originating at the west Florida shelf that are induced by northerly winds. Criteria for determining upwelling and downwelling events can be built strictly for duration, the time period between consecutive events and strength. This would improve characteristics of upwelling and downwelling. Also, it is possible to establish tracer experiments by introducing potential sources at different locations in the study domain in order to examine spatial extent of particles on the surface as well as in the near-bottom layer, and to better estimate risk of pollution hazards for the northeastern Gulf of Mexico as well as for the entire Gulf of Mexico.

APPENDIX A

SEA SURFACE HEIGHT, TEMPERATURE AND TEMPERATURE ANOMALY ALONG THE CROSS-SECTION 88.5 °W

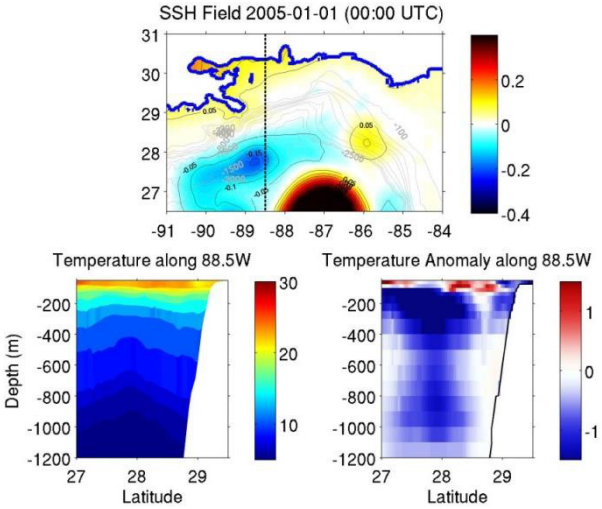

Figure A-1: Upper figure is a snapshot of demeaned SSH on 1 January (2005 or simulation year 14) (00:00 UTC). The dashed line indicates a meridional cross section at 88.5°W; hot color and solid contour represent positive SSH anomalies; cold color and dashed contours are negative SSH anomalies. Lower figures show temperature (°C) (left) and temperature anomaly (°C) (right) along the cross-section.

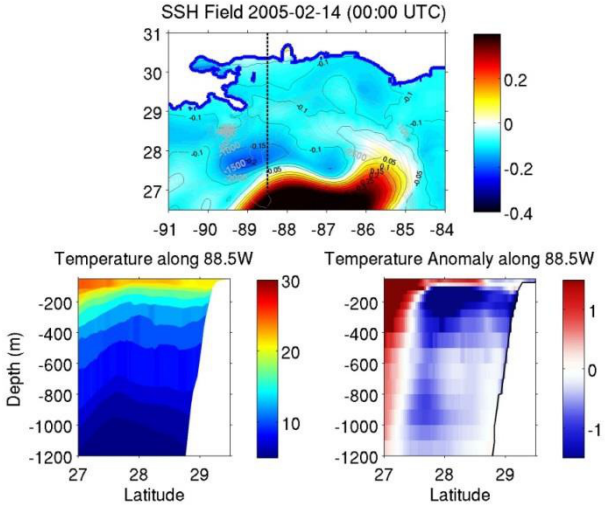

Figure A-2: Upper figure is a snapshot of demeaned SSH on 14 February (2005 or simulation year 14) (00:00 UTC). The dashed line indicates a meridional cross section at 88.5°W; hot color and solid contour represent positive SSH anomalies; cold color and dashed contour are negative SSH anomalies. Lower figures show temperature (°C) (left) and temperature anomaly (°C) (right) along the cross-section.

APPENDIX B

HOVMÖLLER DIAGRAMS OF SSH ANOMALY ALONG THE ISOBATHS

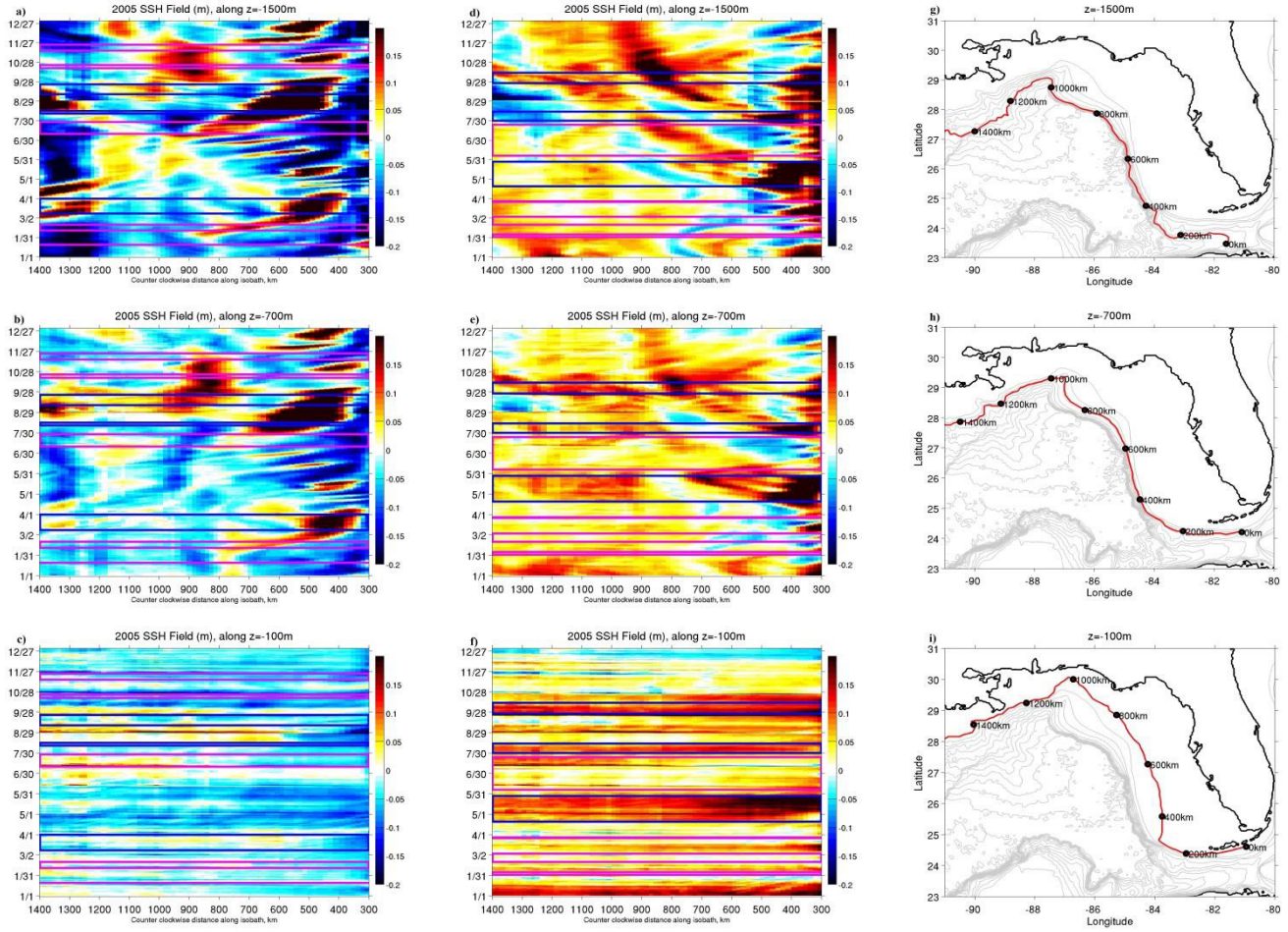

Figure B-1: Hovmöller diagrams of SSH anomaly along the 100, 700 and 1500 m isobaths in simulation year 14 (a, b, c) and year 32 (d, e, f). Color indicates SSH anomaly. The horizontal axis is the distance along the isobaths and the vertical axis is the date ranging from 1 January to 31 December. Maps of distance along the isobaths (g, h, i). The pink/blue boxes indicate upwelling/downwelling periods.

APPENDIX C

NORMALIZED HISTOGRAMS OF VERTICAL EXCURSION FOR INTERFACES 15 AND 18

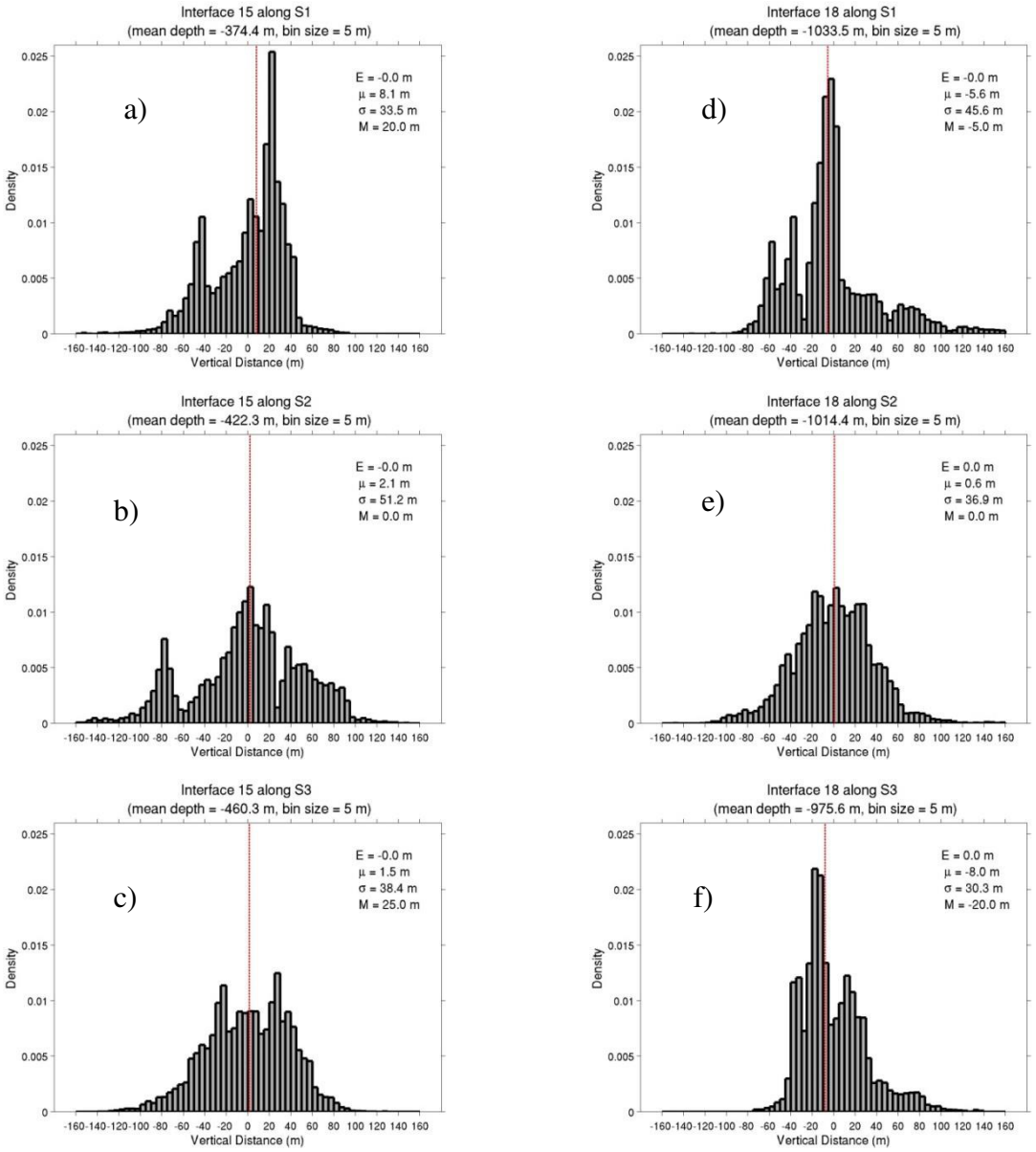

Figure C-1: Normalized histograms of vertical excursion of interfaces 15 (a, b, c) and 18 (d, e, f) at sections S1, S2 and S3 with a bin size of 5 m. The dashed red line indicates the median; E is mean value, μ is the median, σ is standard deviation and M is the mode. Horizontal and vertical axes are vertical distance in meters and probability density, respectively.

APPENDIX D

NORMALIZED HISTOGRAMS OF UPWELLING AND DOWNWELLING DURATION FOR INTERFACES 15 AND 18

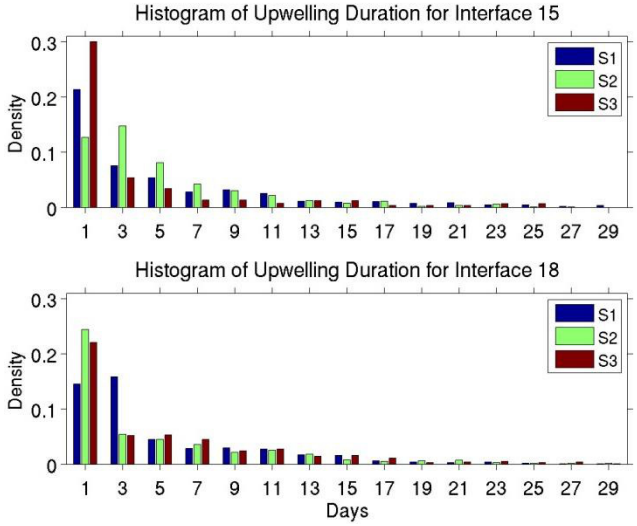

Figure D-1: Normalized histograms of upwelling duration for interfaces 15 (upper) and 18 (lower). Horizontal and vertical axes indicate duration in days and probability density, respectively.

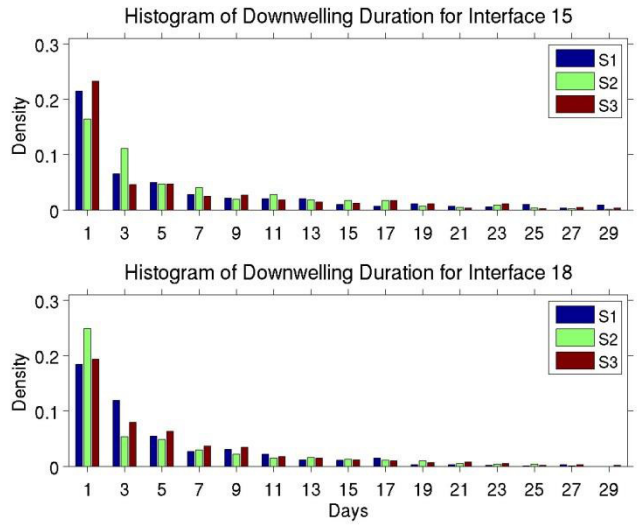

Figure D-2: Normalized histograms of downwelling duration for interfaces 15 (upper) and 18 (lower). Horizontal and vertical axes indicate duration in days and probability density, respectively.

REFERENCES

Abbott, M. R. and P. M Zion (1987), Spatial and temporal variability of phytoplankton pigment off northern California during Coastal Ocean Dynamics Experiment 1. *J. Geophys. Res., 92*, doi: 10.1029/JC092iC02p01745.

Abbott, M. R., and B. Barksdale (1991), Phytoplankton pigment patterns and wind forcing off central California. *J. Geophys. Res., 96* (C8), 14649–14667.

Adelson, J. (2012), About 565,000 pounds of oiled material from Deepwater Horizon stirred up by Hurricane Isaac. The Times-Picayune. http://www.nola.com/news/gulf-oil-spill/index.ssf/2012/10/about_565000_lbs_of_oiled_mate.html.

Allen, S. E. (1996), Topographically generated, sub-inertial flows within a finite length canyon. *J. Phys. Oceanogr., 26*, 1608–1632.

Bakun, A. (1993), The California Current, Benguela Current, and Southwestern Atlantic Shelf Ecosystem: A comparative approach to identifying factors regulating biomass yields1 in: *Large Marine Ecosystem: Stress, Mitigation and Sustainability*, edited by Sherman, K., L. M. Alexander, B. D. Gold, 199–221, AAAS, Washington D.C., U.S.

Bleck, R., C. Rooth, D. Hu, and L. Smith (1992), Salinity-driven thermocline transients in a wind- and thermohaline-forced isopycnic coordinate model of the North Atlantic. *J. Phys. Oceanogr., 22*, 1486–1505.

Boyer, D. L., D. B. Haidvogel, and N. Perenne (2004), Laboratory numerical model comparisons of canyon flows: A parameter study. *J. Phys. Oceanogr., 34*, 1588–1609.

Brink, K. H., F. F. G. Abrantes, P. A. Bernal, R. C. Dugdale, M. Estrada, L. Hutchings, R. A. Jahnke, P. J. Müller, and R. L. Smith (1995), How do coastal upwelling systems operate as integrated physical, chemical, and biological systems and influence the geological record? The role of physical processes in defining the spatial structures of biological and chemical variables, in *Upwelling in the Ocean-Modern Processes and Ancient Records*, edited by C. P. Summerhayes et al., 103 – 124, John Wiley, New York.

Chapman, D. C., and K. H. Brink (1987), Shelf and slope circulation induced by fluctuating offshore forcing. *J. Geophys. Res., 92* (11), 741–759.

Chassignet, E. P., L. T. Smith, G. R. Halliwell, and R. Bleck (2003), North Atlantic simulation with the HYbrid Coordinate Ocean Model (HYCOM): Impact of the vertical coordinate choice, reference density, and thermobaricity. *J. Phys. Oceanogr., 33*, 2504–2526.

Chassignet, E. P. H. E. Hurlburt, O. M Smedstad, G. R. Halliwell, A. J. Wallcraft, E. J. Metzger, B. O. Blanton, C. Lozano, D. B. Rao, P. J. Hogan, and A. Srinivasan (2006), Generalized vertical coordinates for eddy-resolving global and coastal ocean forecasts. *Oceanography, 19*(1), 118–129.

Clarke, A. J. (1977), Observational and numerical evidence for wind-forced coastal-trapped long waves. *J. Phys. Oceanogr., 7*, 231–247.

Collard, S. B. and A. Lugo-Fernandez (1999), Coastal upwelling and mass mortalities of fishes and invertebrates in the northeastern Gulf of Mexico during spring and summer 1998. OSC Study MMS 99-0049. U.S. Department of the Interior, Minerals Management Service, Gulf of Mexico OCS Region, New Orleans, LA.

Collard, S. B., G. Fitzhugh, J. Brusher and R. Shaffer (2000), A mass mortality event in coastal waters of the central Florida Panhandle during spring and summer 1998. *Gulf Mex. Sci. 18*, 68–71.

Coria-Monter, E., M. A. Monreal-Gómez, D. A. Salas-de-León, J. Aldeco-Ramírez, and M. Merino-Ibarra (2014), Differential distribution of diatoms and dinoflagellates in a cyclonic eddy confined in the Bay of La Paz, Gulf of California. *J. Geophys. Res.* – Oceans, doi: 10.1002/2014JC009916.

Cragg, J., G. Mitchum, and W. Sturges (1983), Wind-induced sea-surface slopes on the west Florida shelf. *J. Phys. Oceanogr., 13*, 2201–2212.

Csanady, G. T. (1978), The arrested topographic wave. *J. Phys. Oceanogr., 8*, 47–62.

Day, J., P. templet, JY. Ko, W. Mitsch, G. P. Kemp, J. Johnston, G. Steye, J. Barra, D. Justic, E. Clairain, and R. Theriot (2004), *The Mississippi Delta: System functioning, environmental impacts and sustainable management*. Environmental analysis of the Gulf of Mexico. Harte Research Institute for the Gulf of Mexico Studies Special Publication Series No. 1. Editor: K. Withers and M. Nipper.

Dukhovskoy, D. S., R. R. Leben, E. P. Chassignet, S. L. Morey and R. Nedbor-Gross (2014), Characterization of the uncertainty of the Loop Current Metrics using a multi-decadal numerical simulation and altimeter observations. *Deep-Sea Res. Part 1* (in review).

Fernandez-Partagas, J., and C. N. Mooers (1975), A subsynoptic study of winter cold fronts in Florida. Mon. *Wea. Rev., 10*3, 742–744.

Forristal, G. Z., K. J. Schaudt, and C. K. Cooper (1992), Evolution and kinematics of a Loop Current eddy in the Gulf of Mexico during 1985. *J. Geophys. Res., 97*, 2173–2184.

Freeland, H., and K. Denman (1982), A topographically controlled upwelling center off southern Vancouver Island. *Journal of Marine Research, 40*, 1069–1093.

Garcia-Reyes, M., J. L. Largier, and W. J. Sydeman (2014), Synoptic-scale upwelling indices and predictions of phyto- and zooplankton populations. *Progress in Oceanography, 120*, 177–188.

Gill, A. E., and A. J. Clarke (1974), Wind-induced upwelling, coastal currents and sea-level changes. *Deep Sea Res., 21*, 325–345.

Gill, A. E., and E. H. Schumann (1974), The generation of long shelf waves by the wind. *J. Phys. Oceanogr., 4*, 83–90.

Haidvogel, D. B. (2004), Cross-shelf exchange driven by oscillatory barotropic currents at an idealized coastal canyon. *J. Phys. Oceanogr., 35*, 1054–1067.

Haidvogel, D. B., A. Beckmann, and K. S. Hedström (1991), Dynamical simulations of filament formation and evolution in the Coastal Transition Zone. *J. Geophys. Res., 96*, doi: 10.1029/91JC00943.

Hamilton, P. and A. Lugo-Fernandez (2001), Observations of high speed deep currents in the northern Gulf of Mexico. *Geophys. Res. Letters, 28* (14), 2867–2870.

Hamilton, P. and T. N. Lee (2005), Eddies and jets over the slope of the northeast Gulf of Mexico. *Circulation in the Gulf of Mexico: Observations and Models*. *Geophysical Monograph Series 161*, 123–142.

He, R., and R. H. Weisberg (2003), A Loop Current intrusion case study on the west Florida shelf. Notes and Correspondence. *J. Phys. Oceanogr*., 465–477.

Hetland, R. D. (1999), The dynamics of a Loop Current forced shelf break jet on the west Florida shelf, PhD dissertation, 77 pp., Florida State University, Tallahassee, 12 April.

Hetland, R. D., R. R. Leben and P. P. Niiler (1999), A Loop Current-induced jet along the edge of the west Florida Shelf. *Geophys. Res. Letters, 26* (15), 2239–2242.

Hickey, B. (1997), The response of a steep-sided, narrow canyon to time-variable wind forcing. *J. Phys Oceanogr., 27*, 697–726.

Hine, A. C., S. C. Dunn, and S. D. Locker (2013), Geologic beginnings of the Gulf of Mexico with emphasis on the formation of the DeSoto Canyon. http://deep-c.org/news-and-multimedia/in-the-news/geologic-beginnings-of-the-gulf-of-mexico-with-emphasis-on-the-formation-of-the-de-soto-canyon.

Holton, J. R. (1992), *An Introduction to Dynamic Meteorology*. 3rd edition, 511pp.

Hopkinson, C. (2010). Outcome/guidance from Georgia Sea Grant Program: Current status of BP oil spill. Georgia Sea Grant report on August 17, 2010, 5pp.

Hsu, S. A. (1999), Marine meteorology and air-sea interactions over the DeSoto Canyon and adjacent shelf. *Physical/Biological Oceanographic Integration Workshop for the DeSoto Canyon and Adjacent Shelf*, edited by Schroeder W. W., and C. F. Wood. OCS Study Minerals Management Service 2000-074.

Hsueh, Y., G. O. Marmorino, and L. Vansant (1982), Numerical model studies of the winter-storm response of the west Florida shelf. *J. Phys. Oceanogr., 12*, 1037–1050.

Hsueh, Y., and Y., Golubev (2002), A numerical model calculation of the flow in DeSoto Canyon in response to northerly wind bursts in winter. *Gulf of Mexico Science*, 44–59.

Hsueh, Y., and R. Weisberg (2002). Northeastern Gulf of Mexico. Final Report. OCS Study MMS 2002-053.

Huh, O. K., W. J. Wiseman, and L. J. Rouse (1981), Intrusion of Loop Current waters onto the west Florida shelf. *J. Geophys. Res., 86*, 4186–4192.

HYCOM user's guide (2003): https://hycom.org/attachments/063_hycom_users_guide.pdf

Kämpf, J. (2007), On the magnitude of upwelling fluxes in shelf-break canyons. *Continental Shelf Research, 27*, 2211–2223.

Klinck, J. (1996), Circulation near submarine canyons: A modeling study. *J. Geophys. Res., 101*(C1), 1211–1223.

Ko, JY., J. Day, J. Barras, R. Morton, J. Johnston, G. Steyer, G. P. Kemp, E. Clairain and R. Theriot (2004), Impacts of oil and gas activities on coastal wetland loss in the Mississippi Delta. Environmental Analysis of the Gulf of Mexico. Harte Research Institute for the Gulf of Mexico Studies Special Publication Series No. 1. Editor: K. Withers and M. Nipper.

Koblinksky, C. J., and P. P. Niiler (1980), Direct measurements of circulation on west Florida continental shelf, January 1973 – May 1975. *Data Rep. 76*, Ref. 7 –13, 102 pp., School of Oceanogr., Oreg. State Uni..

Leben, R. R. (2005), Altimeter-derived Loop Current metrics. *Circulation in the Gulf of Mexico: Observations and Models. Geophysical Monograph Series 161*, 181–201.

Li, Z. and R. H. Weisberg (1999), West Florida shelf response to upwelling favorable wind forcing: Kinematics. *J. Geophys. Res. 104*(C6), 13507–13527.

Maksimova, E. V. and A. J. Clarke (2013), Multiyear subinertial and seasonal Eulerian current observations near the Florida Big Bend coast. *American Meteorological Society*, 1691–1709.

Marmorino, Go. O. (1982), Wind-forced sea level variability along the west Florida shelf (winter, 1978). *J. Phys. Oceanogra., 12*, 389–405.

Marmorino, G. O. (1983), Variability of current, temperature, and bottom pressure across the west Florida continental shelf, winter, 1981-1982. *J. Geophys. Res., 88*(C7), 4439–4457.

Mirshak, R., and S. E. Allen (2005), Spin-up and the effects of a submarine canyon: Application to upwelling in Astoria Canyon. *J. Geophys. Res., 110*, C02013, doi: 10.1029/2004JC002578.

Mitchum, T. G., and A. J. Clarke (1986), Evaluation of frictional, wind forced long wave theory on the west Florida shelf. *J. Phys. Oceanogr., 16,* 1029–1037.

Mitchum, T. G., and W. Sturges (1982), Wind-driven currents on the west Florida shelf. *J. Phys. Oceanogr., 12*, 1310–1317.

Moeller, C. C., O. K. Huh, H. H. Roberts, L. E. Gumley and N. P. Menzel (1993), Response of Louisiana coastal environments to a cold front passage. *Journal of Coastal Research, 9* (2), 434–447.

Morey, S. L., J. Zavala-Hidalgo and J. J. O'Brien (2005), The seasonal variability of continental shelf circulation in the Northern and Western Gulf of Mexico from a high-resolution numerical model. *Circulation in the Gulf of Mexico: Observations and Models. Geophysical Monograph Series 161*, 203–218.

Muller, R. A. (1977), A synoptic climatology for environmental baseline analysis: New Orleans. *J. Appl. Meteor., 16*, 20–33.

Muller, R. A. and J. E. Willis (1983), New Orleans weather 1961-1980: A climatology by means of synoptic weather types. *Misc. Pub. 83-1*, School of Geoscience, Louisiana State University, Baton Rouge.

Muller-Karger, F. E., F. Vukovich, R. Leben, B. Nababan, C. Hu, and D. Myhre (2000), Remote sensing study of upwelling in the northeastern Gulf of Mexico and the effects of hurricanes Earl and Georges. Annual Report: Year 2. U.S. Department of the Interior, Minerals Management Service, Gulf of Mexico OCS Region, New Orleans, LA. OCS Study MMS 2000, 42 pp.

Nowlin, W. D. Jr., A. E. Jochens, M. K. Howard, S. F. DiMarco, and W. W. Schroeder (2000), Hydrographic properties and inferred circulation over the northeaster shelves of the Gulf of Mexico during spring to midsummer of 1998. *Gulf of Mexico Science, 2000* (1), 40–54.

Oey, L. Y., T. Ezer, and H. C. Lee (2005), Loop Current, rings and related circulation in the Gulf of Mexico: A review of numerical models and future challenges. *Circulation in the Gulf of Mexico: Observations and Models. Geophysical Monograph Series 161*, 31–56.

Pond, S., and G. L. Pickard (1983), *Introductory Dynamical Oceanography*. 2nd edition, 329pp, Butterworth-Heinemann.

Ramseur, J. L. (2010), Deepwater Horizon oil spill: The fate of the oil. CRS Report for Congress. Congressional Research Service, 7-5700.

Raynie, R. C., and S. K. Beasley (2000), Working to save our coastal wetlands. Public information brochure. Baton Rouge, Louisiana: Louisiana Department of Natural Resources, Coastal Restoration Division, 17 pp.

Rosmond, T. E., J. Teixeira, M. Peng, T. F., Hogan, and R. Pauley (2002), Navy operational global atmospheric predictions system (NOGAPS): Forcing for ocean models. *Oceanography, 15*(1), 99–108.

Saha, S., S. Moorthi, H. Pan, X. Wu, J. Wang, S. Nadiga, P. Tripp, R. Kistler, J. Woollen, D. Behringer, H. Liu, D. Stokes, R. Grumbine, G. Gayno, J. Wang, Y. Hou, H. Chuang, H. H. Juang, J. Sela, M. Iredell, R. Treadon, D. Kleist, P. V. Delst, D. Keyser, J. Derber, M. Ek, J. Meng, H. Wei, R. Yang, S. Lord, H. V. D. Dool, A. Kumar, W. Wang, C. Long, M. Chelliah, Y. Xue, B. Huang, J. Schemm, W. Ebisuzaki, R. Lin, P. Xie, M. Chen, S. Zhou, W. Higgins, C. Zou, Q. Liu, Y. Chen, Y. Han, L. Cucurull, R. W. Reynolds, G. Rutledge, and M. Goldberg (2010), The NCEP Climate Forecast System Reanalysis, Bull. *Amer. Meteor. Soc., 91*, 1015–1057, doi: 10.1175/2010Bams3001.1.

She, J., and J. M. Klinck (2000), Flow near submarine canyons driven by constant winds. *J. Geophys. Res. – Oceans, 105*(C12), 28671–28694.

Shi, C., and D. Nof (1993), The splitting of eddies along boundaries. *J. Marine Research, 51*, 771–795.

Smith, R. L. (1968), Upwelling. Oceanogr. *Mar. Biol. Ann. Rev., 6*, 11–46.

Sturges, W., and J. C. Evans (1983), Variability of Loop Current in Gulf of Mexico. *J. Mar. Res., 41*, 639–653, doi: 10.1357/002224083788520487.

Sturges, W. and R. Leben (2000), Frequency of ring separations from the Loop Current in the Gulf of Mexico: A revised estimate. *J. Phys. Oceanogr., 30*, 1814–1819.

Tomczak, M. (1996). Shelf and Coastal Oceanography: http://www.es.flinders.edu.au/~mattom/ShelfCoast/

Vaillancourt, R. D., J. Marra, M. P. Seki, M. L. Parsons, R. R. Bidigare (2003), Impact of a cyclonic eddy on phytoplankton community structure and photosynthetic competency in the subtropical North Pacific Ocean. *Deep-Sea Research Part I, 50*, 829–847.

Vukovich, F. M. (1986), Aspects of the behavior of cold perturbations in the Eastern Gulf of Mexico: A case study. Notes and Correspondence. *American Meteorological Society*, 175–188.

Vukovich, F. M. (2007), Climatology of ocean features in the Gulf of Mexico using satellite remote sensing data. *American Meteorological Society*, 689–707.

Vukovich, F. M. (2012), Changes in the Loop Current's eddy shedding in the period 2001–2010. *International Journal of Oceanography, 2012*, 439042, doi: 10.1155/2012/439042.

Vukovich, F. M., B. W. Crissman, M. Bushnell, and W. J. King (1979), Some aspects of the oceanography of the Gulf of Mexico using satellite and in situ data. *J. Geophys. Res., 84* (C12), 7749–7768.

Walin, G. (1972), On the transient response to meteorological disturbances in the Baltic. *Tellus 24*, No. 3.

Walker, N. D., R. R. Leben and S. Balasubramanian (2005), Hurricane-forced upwelling and chlorophyll a enhancement within cold-core cyclones in the Gulf of Mexico. *Geophys Res. Lett., 32*, L18610, doi: 10.1029/2005GL023716.

Weisberg, R. H. and R. He (2003), Local and deep-ocean forcing contributions to anomalous water properties on the west Florida shelf. *J. Geophys. Res., 108* (C6), 3184, doi:10.1029/2002JC001407.

Weisberg, R. H., Z. Li, and F. E. Muller-Karger (2001), West Florida shelf response to local wind forcing: April 1998. *J. Geophys. Res., 106*, 31239–31262.

Weisberg, R. H., R. He, Y. Liu and J. I. Virmani (2005), West Florida shelf circulation on synoptic, seasonal and interannual time scales. *Circulation in the Gulf of Mexico: Observations and Models. Geophysical Monograph Series 161*, 325–347.

Weisberg, R. H., L. Zheng, Y. Liu, S. Murawski, C. Hu, and J. Paul (2014), Did Deepwater Horizon hydrocarbons transit to the west Florida continental shelf? *Deep-Sea Res. II*, doi: 10.1016/j.dsr2.2014.02.002.

Yang, H., and R. H. Weisberg (1999), Response of the west Florida shelf circulation to climatological wind stress forcing. *J. Geophys. Res., 104*, 5301–5320.

Yocke, M. A., C. A. Emery, P. Roberts, C. MacDonald, D. Ladner, J. Prouty and A. Barnett (2000), Meteorology of the northeastern Gulf of Mexico: Data from 1995 to 1997. Final Report. OSC Study MMS 2000-075.

Yoshida, K., and H. L-. Mao (1957), A theory of upwelling of large horizontal extent. J. Mar. Res., 16, 40–54. Republished in Selected Scientific Papers of Professor Kozo Yoshida, Lab. of Phys. Oceanogr., Geophys. Inst., U. of Tokyo, 1978, 134–148.

Zavala-Hidalgo, J., A. Gallegos-Garcia, B. Martinez-Lopez, S. L. Morey and J. J. O'Brien (2006), Seasonal upwelling on the Western and Southern shelves of the Gulf of Mexico. *Ocean Dynamics*, doi: 10.1007/s10236-006-0072-3.

BIOGRAPHICAL SKETCH

Thanh Tam Nguyen was born and raised in Hanoi, Vietnam. She graduated with Honors Bachelor of Science in oceanography from College of Science, Vietnam National University in 2007. Then she worked for governmental research organizations in Vietnam for two years and attended a Master's program in coastal engineering at Delft University of Technology in the Netherlands in 2009. Right after graduation, she moved to Tallahassee, Florida to start a graduate program in physical oceanography at Florida State University and defended her second Master's thesis in the Fall of 2014.